ADVANCED MATERIALS
www.advmat.de

Revisiting the Nature of Chemical Bonding in Chalcogenides to Explain and Design their Properties

Matthias Wuttig, Carl-Friedrich Schön, Jakob Lötfering, Pavlo Golub, Carlo Gatti, and Jean-Yves Raty*

Quantum chemical bonding descriptors have recently been utilized to design materials with tailored properties. Their usage to facilitate a quantitative description of bonding in chalcogenides as well as the transition between different bonding mechanisms is reviewed. More importantly, these descriptors can also be employed as property predictors for several important material characteristics, including optical and transport properties. Hence, these quantum chemical bonding descriptors can be utilized to tailor material properties of chalcogenides relevant for thermoelectrics, photovoltaics, and phase-change memories. Relating material properties to bonding mechanisms also shows that there is a class of materials, which are characterized by unconventional properties such as a pronounced anharmonicity, a large chemical bond polarizability, and strong optical absorption. This unusual property portfolio is attributed to a novel bonding mechanism, fundamentally different from ionic, metallic, and covalent bonding, which is called "metavalent." In the concluding section, a number of promising research directions are sketched, which explore the nature of the property changes upon changing bonding mechanism and extend the concept of quantum chemical property predictors to more complex compounds.

1. Outline and Goals of this Review

In the last decade, material science has witnessed the rise of several novel classes of advanced functional materials, including halide perovskite-based solar absorbers, topological insulators, and hydrides for high-temperature superconductivity.[1–10] Frequently, these materials have demonstrated properties which compete or even surpass the best previously known materials for these applications. Given the industrial significance of solar absorbers and superconductors as well as the potential impact of topological insulators, one can wonder how these novel contenders were found. Clearly, chemical intuition and ingenuity played an important role, as well as the growing understanding of the role of topology for material properties. Yet, one should even ponder about a rather different question. Given the significance of the applications mentioned above, why did it take so long to identify these new compounds.

After all, many scientists strive to design advanced functional materials.[11] This holds, e.g., for thermoelectrics, which transform thermal into electrical energy and vice versa, solar cell absorbers, which convert photon energy into electrical energy, and phase-change materials (PCMs), where the reversible phase transition from the amorphous to the crystalline phase is utilized to store information.[12] For all of these application scenarios, scientists look to identify materials with tailored functionalities. In recent years, vast databases have been built to excel the identification of superior

M. Wuttig, C.-F. Schön, J. Lötfering
I. Institute of Physics
Physics of Novel Materials
RWTH Aachen University
52056 Aachen, Germany
E-mail: wuttig@physik.rwth-aachen.de
M. Wuttig
Jülich-Aachen Research Alliance (JARA FIT and JARA HPC)
RWTH Aachen University
52056 Aachen, Germany
The ORCID identification number(s) for the author(s) of this article can be found under https://doi.org/10.1002/adma.202208485.

DOI: 10.1002/adma.202208485

M. Wuttig
PGI 10 (Green IT)
Forschungszentrum Jülich GmbH
52428 Jülich, Germany
P. Golub
Department of Theoretical Chemistry
J. Heyrovský Institute of Physical Chemistry
Dolejškova 2155/3, Prague 8 182 23, Czech Republic
C. Gatti
CNR-SCITEC
Istituto di Scienze e Tecnologie Chimiche "Giulio Natta"
sezione di via Golgi
via Golgi 19, Milano 20133, Italy
J.-Y. Raty
CESAM B5
Université de Liège
Sart-Tilman B4000, Belgium

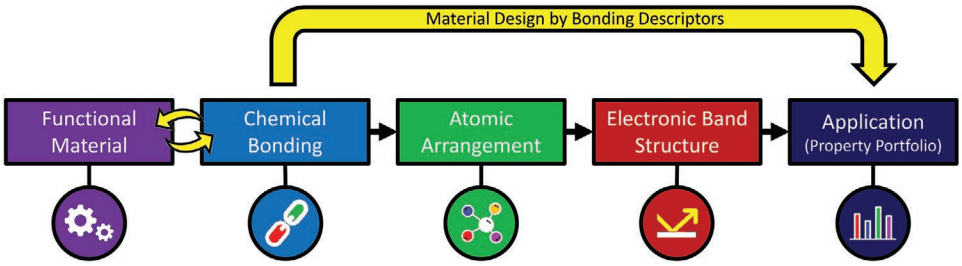

Figure 1. Employing chemical bonding descriptors to design functional materials. The properties of solids depend upon their chemical bonding type. Chemical bonding and atomic arrangement are closely related and have a profound impact on the resulting electronic band structure, which governs many properties of functional materials. The property portfolio of a functional material on the other hand defines its application potential. This close interdependence can be employed to design materials with targeted functionalities by exploiting appropriate quantum chemical bonding descriptors, which hence are utilized as property predictors. Adapted under the terms of the CC-BY Creative Commons Attribution 4.0 International license (https://creativecommons.org/licenses/by/4.0).[80] Copyright 2022, The Authors, published by American Society for the Advancement of Science.

materials.[13,14] Combinatorial synthesis creating huge material libraries and machine learning have been employed to identify tailored functional materials.[15]

Usually, advanced functional materials like PCMs or superior solar cell absorbers are discussed in terms of their band structure and the resulting properties. Here, we will review a rather different approach and its potential to design advanced functional materials focusing on a group of chalcogenides with an unconventional portfolio of properties. It will be argued that a quantification of chemical bonding provides the metric to describe systematic trends in the resulting material properties. The close interrelation between precise quantum chemical bonding descriptors and materials properties hence enables the application of these descriptors as property predictors. This is sketched in **Figure 1**.

To reach this goal, we will first discuss disputes in developing a consistent understanding of chemical bonding in the last hundred years, i.e., after the advent of quantum mechanics and the Schrödinger equation.[16] Reviewing these differences and controversies can help to comprehend the reluctance of many material scientists to use concepts of chemical bonding to understand, unravel, or tailor material properties. We will close the second section with a discussion on recent disagreements on the bonding mechanism employed in several chalcogenides, a class of materials with an interesting portfolio of applications ranging from thermoelectric energy converters to PCMs and topological insulators.

In Section 3, recent advances in quantum chemical calculations are reviewed. The concepts developed provide the necessary tools for an unambiguous description and quantification of chemical bonds. These tools, in particular the localization and delocalization index (LI and DI), and several quantities derived from those, as well as the domain averaged Fermi hole, will be utilized to settle the controversies on unconventional bonding mechanisms in several chalcogenides. It will be shown that these bonding descriptors provide a coherent view on bonding in these and other solids. Indeed, they can be employed to construct a simple, yet powerful map which explains and predicts important property trends for advanced functional materials. This map will be presented and discussed in Section 4, where it will also be compared with previous generations of material maps and their respective advantages and disadvantages.

In Section 5, the quantum chemical bonding descriptors will be employed to explain relevant material properties. In this section, we will focus on a growing set of technological relevant chalcogenides. This happens for two reasons. It will first be presented how their unconventional properties can be related to their unusual bonding mechanism. Second, it will be shown that this bonding mechanism is distinctively different from well-known metallic, ionic, and covalent bonding. It has hence been suggested to call the bonding "metavalent" bonding. The reasons for the introduction of a novel bonding mechanism besides the aforementioned types will also be reviewed in this section. In Section 6, we will briefly discuss why it seems advantageous or even mandatory to introduce metavalent bonding as a novel and fundamental bonding mechanism, instead of describing it as a subset of covalent bonding or alternatively as a mixture of covalent and metallic bonding. In this chapter, also competing bonding mechanisms will be discussed, which have been suggested to explain these chalcogenides, including electron-rich hypervalent bonding, resonant bonding, and the potential impact of lone pairs. In Section 7, uncharted opportunities as well as challenges for the design approach presented here will be discussed, followed by a short summary.

2. Chemical Bonding in Solids: Past and Present Controversies

Soon after the advent of quantum mechanics, its relevance to describe and understand chemical bonding became apparent.[16] Indeed, in the first decades after the Schrödinger equation was established, significant progress was made in unraveling the origin of covalent bonding. Linus Pauling's book on the nature of the chemical bond has summarized much of this progress made in those days.[17] The book and its author have shaped the thinking of generations of scientists. Yet, at the same time, Pauling was also involved in heated controversies in an opinion-forming capacity. The debates about the valence bond (VB) versus molecular orbital (MO) interpretation of covalent bonds have influenced the community of chemists for decades.[18–22] However, the controversies did not end there; mainly because the problem is more fundamental in nature than the competition between two alternative and fictitious interpretive models, which are based on different combinations of single

one-electron orbitals. Yet, these models have been shown to be fully equivalent when taken in their converged forms.

Indeed, the underlying problem is twofold. Solving the Schrödinger equation for a large system size is increasing dramatically in complexity with increasing electron number. Yet, even if we could solve the Schrödinger equation for such a complex system, the amount of information stored in the wavefunction Ψ escapes existing storage capacities and human comprehension.[23,24] Thus, the use of information compression techniques is mandatory. Two distinctively different paths are usually followed.[25] In the first path, models and approximations used to solve Schrödinger's equation, are also exploited to rationalize Ψ. For instance, within the Hartree–Fock approximation, Ψ is written as a single determinant constructed from one-electron functions or orbitals. Electrons move, in a mean-field approach, in the average potential created by the remaining particles of the system. One-electron orbital-based descriptions, such as MOs and VB orbitals, are thus customarily adopted to discuss bonding, since the knowledge and manipulation of *N* 3D functions is much easier to realize than that of Ψ. However, this simplification comes at the expense of several problems and caveats. Orbitals are not unique, due to the infinite number of possible transformations that leave the total Ψ invariant. Furthermore, they are also largely method-dependent. In addition, when the mean-field is abandoned, and electron correlation is taken into account, the single determinant orbital concept breaks down and significantly more than *N* partially occupied functions appear. The simple MO machinery, or the simple single configuration VB approach, thus ceases to be adequate.

In the second path that is followed alternatively, the information contained in the wavefunction Ψ is instead compressed using its probabilistic interpretation. This leads to probability densities of finding electrons or electron pairs at given positions of space (or with given momenta). These "reduced densities", as they are known, are quantum mechanical observables. They are invariant under orbital transformations, do not depend, by definition, on models or computational methods and can be experimentally accessed. From such probability densities, a vast number of physically unbiased descriptors can be retrieved. These descriptors can be employed to discuss chemical bonding and the ensuing system's or material's properties. They are the ingredients of the family of the increasingly popular quantum chemical topological (QCT) approaches.[26] Bader's quantum theory of atoms in molecule (QTAIM) is presumably the most representative of them.[27] The well-known empirical paradigms of chemistry, including chemical bonds, chemical groups, and their transferable properties as well as the idea of shared and isolated electron pairs can thus be related to manageable mathematical objects. This approach is not restricted to molecules and has been extended to solids in the last 35 years.[28–33]

Interpretive tools such as COOP (crystal orbital overlap population) and COHP (crystal orbital Hamilton population) for solids,[34,35] based on single-particle electron states and going beyond their usual Bloch function-based delocalized representation, lead to different mathematical objects. Yet, they serve similar (and sometimes complementary) purposes to those defined within the QCT approaches. They often produce compatible views. This is not surprising, since both are derived from the same underlying Ψ. The main difference between orbital-based and QCT descriptors lies, respectively, in their fictitious or physical nature. This advantage might suffice to convince employing the QCT-based approach. Since the one-electron density is an observable, most QCT descriptors can even be obtained from experiment.[29,30,36–39] So it comes as no surprise that for five decades X-ray electron density analysis has investigated hundreds and hundreds of materials, often using QTAIM and other QCT approaches to characterize their bonding features and interpret their properties.[30,36,40,41] Yet, the orbital view has been the method of choice in chemistry for several generations, providing interpretative tools, which are not rapidly abandoned. COOP and COHP methods, for instance, provide to chemists an energy-resolved picture of chemical bonding, highlighting the bonding and antibonding character of orbitals in solids. Alternatively, the hybridization concept, with its supposed chemical bonding implication, can be nicely explored by the generalization to the solid state of the natural bond orbital method.[42] Maximally localized orbitals (Wannier/Boys), on the other hand, yield the most compact set of orbitals that describe an entire system, from large molecules to periodic solids.[43] Such orbitals are often envisaged as eye-catching, qualitative representations of individual chemical bonds.

Nevertheless, Hoffmann provocatively observed in 1988 that "many solid-state chemists have isolated themselves from their organic or even inorganic colleagues by choosing not to see bonds in their materials."[44] Solid-state physicists usually refrain from quantifying chemical bonding using sophisticated quantum-chemical tools, but instead focus on the atomic arrangement and the resulting electronic band structure to explain material properties. Even the very notion of chemical bonds has recently been debated.[45]

Yet, there are a number of advanced functional materials where concepts of chemical bonding have been invoked to explain unconventional material properties. This holds for IV–VI semiconductors, e.g., which are employed as thermoelectrics and PCMs. Material scientists already noted more than 40 years ago that these compounds encompass unusual properties. They behave very different from the more familiar III–V or II–VI semiconductors such as GaAs or ZnSe. This holds for the pressure dependence of the energy gap, the electronic structure, and the static dielectric constant.[46] Hence, scientists have attempted to attribute these properties to differences in their bonding mechanisms. Surprisingly, a few rather different bond types have been suggested to govern these monochalcogenides, as summarized in **Table 1**. We will focus in the following first on cubic GeTe and later generalize the conclusions derived for other cubic and rhombohedral IV–VI monochalcogenides. Frequently, GeTe is discussed in analogy with PbTe as a material where the Ge lone pair s electrons play a prominent role. In this view, GeTe is described as an ionic material, where the occupied Ge $4s^2$ state also influences material properties. In other studies, GeTe is described as a solid with ten valence electrons. In this picture, it is assumed that all formal valence electrons, i.e., the two outermost s electrons of both Ge and Te contribute to bond formation, as well as the two outermost p electrons of Ge and the four outermost p electrons of Te. On the contrary, metavalent bonding, a recently introduced bonding scheme, assumes that only the two outermost p electrons of Ge

Table 1. Bonding schemes suggested for IV–VI semiconductors like cubic GeTe (or PbTe). The table lists the number of electrons involved in bonding for the IV–VI compound, specifies these electrons and provides the name given to this bonding scheme.

Number of electrons involved in bonding	Bonding Scheme	Electrons involved in bonding
12 e	Hypervalent (3c–4e)	??
10 e	"10 electron solids"	Ge $4s^2$ $4p^2$ Te $5s^2$ $5p^4$
8 e	Lone pair involved	Ge $4s^2$ $4p^2$ Te $5p^4$
6 e	Metavalent (2c–1e)	Ge $4p^2$ Te $5p^4$

and the four outermost p electrons of Te contribute to bond formation. Hence, in total only six electrons are available for bond formation. Given the fact that the atoms in cubic GeTe have six nearest neighbors, with such a small number of bonding electrons, only electron-deficient bonds can be formed. We note in passing that in the past the term resonant bonding has been invoked for crystalline PCMs like GeTe or $Ge_2Sb_2Te_5$. The drawbacks of the phrase resonant bonding for PCMs will be discussed in Section 6.[47–49] Finally, materials like cubic GeTe and $Ge_2Sb_2Te_5$ have recently been described as electron-rich, forming hypervalent multicenter bonds.[50,51] Specifically, it has been suggested that these compounds form 3c–4e bonds. Since PbTe and GeTe have three orthogonal bond axes, in total 12 electrons would be needed to form three orthogonal hypervalent bonds. So far, it has not been explained, which orbitals provide the 12 electrons required to form these bonds.

It is fascinating that for these IV–VI compounds with simple crystal structure, such a large variety of different bonding mechanisms have been suggested. What is particularly striking is the difference in the number of electrons involved in bond formation for these models. This divergence of views seems to indicate that it is very challenging to clarify the bonding mechanism between adjacent atoms. In any case, it might be insightful to try to understand its origin and resolve the controversy created by the contradicting bonding mechanisms. To this end, we will focus on cubic GeTe but also present similar data for rhombohedral GeTe, a PCM, in the Supporting Information. It should be noted that cubic GeTe is a model system which is unstable toward its rhombohedral phase. Hence, we will also discuss if and how the bonding changes upon increasing rhombohedral distortion.

To clarify which electrons contribute to bonding, the orbital resolved density of states (DoS) can be analyzed. This quantity can be obtained from the band structure upon projection on the different orbitals. The orbital-resolved DoS has been determined with Quantum Espresso.[52,53] The resulting data for the integrated orbital-resolved density of states (IDOS) are depicted in **Figure 2**. Electrons from adjacent atoms, which participate in an "electron pair," overlap with each other. Overlap of orbitals leads to a dispersion of the corresponding bands, which is reflected in the DoS. With this argument in mind, one can see that there is a steep (instantaneous increase) in the density of the d states of Ge and Te. There is hence no overlap of d orbitals with other orbitals, including d orbitals from any adjacent atom. These d orbitals are also completely filled far below the Fermi energy E_F with ten electrons each. They are thus not

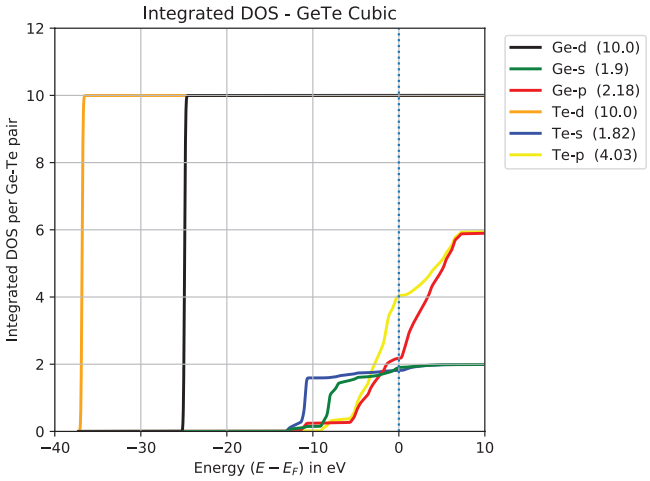

Figure 2. Orbital resolved integrated density of states for the cubic (*Fm3m*) phase of GeTe. The density of states is projected onto the orbital contributions of each element and numerically integrated from $-\infty$ to the respective energy value on the *x*-axis. This value then corresponds to the total number of electrons within that orbital up this energy level.

involved in electron pair formation and hence bonding. Subsequently, the Te s state appears, starting to increase considerably at about –12 eV below E_F, while the Ge s state starts to rise at about –8 eV below E_F. Yet, they are also almost completely filled, as obtained upon integrating the orbital-resolved DOS of the corresponding state up to E_F. The occupation of the s states of Te and Ge corresponds to 1.82 and 1.90 s electrons, respectively. Hence, it is not clear, if these s electrons significantly contribute to bonding. The p electrons of Ge and Te only start to be filled considerably at about 4.1 eV below E_F. There is still a large fraction of empty states of both Te and Ge above the Fermi level. Hence, the p electrons seem to play the prominent role for bonding. On the contrary, the role of the s electrons is not completely clear from an inspection of the DoS. This ambiguity can possibly help to understand the different views on bond formation that is apparent from Table 1. For comparison, also the distribution of the formal valence electrons over the outermost Ge and Te states is shown for the rhombohedral (*R3m*) and orthorhombic (*Pnma*) phase of GeTe as well. The occupation of these states does not show pronounced differences, demonstrating that the integrated DoS does not change significantly upon changes of atomic arrangement and bonding. In the Supporting Information, the orbital-resolved DoS is shown for Si, where a significant fraction of Si 3s and 3p states are both occupied and empty, in contrast to cubic GeTe, indicating that for Si both the outermost s and p orbitals contribute to bond formation.

The discussion presented above as well as the data in **Table 2** is not compatible with the formation of hypervalent bonds, where three centers are held together by four electrons. Since GeTe forms bonds in three almost perpendicular directions, three such hypervalent bonds would have to be formed requiring 12 electrons. Table 2 and Figure 1 show that the number of electrons available is insufficient to form these three hypervalent bonds. Instead, the orbital-resolved DoS is fully compatible with the metavalent bonding mechanism in Table 1, since only the p states have both a significant fraction of filled and empty states

Table 2. Occupation of the Ge 4s and 4p states, as well as the Te 5s and 5p states for three different phases of GeTe obtained from the orbital resolved integrated DOS (see the Supporting Information). Both Ge and Te s states are occupied almost completely, with close to 2 electrons; while the Ge and Te p states are only partially occupied with about 2 and 4 electrons, respectively. No major difference is seen for the three different phases of GeTe. The sum of the projected DOS on all states does not add up to 10 (number of formal valence electrons), since the basis that is used for projection is not complete as higher energy states are not considered.

Phase	Ge 4s state	Ge 4p state	Te 5s state	Te 5p state	Sum p states	Sum all states
Cubic (*Fm3m*)	1.90 e	2.18 e	1.82 e	4.03 e	6.21	9.93 e
Rhombohedral (*R3m*)	1.88 e	2.15 e	1.79 e	4.12 e	6.27	9.94 e
Orthorhombic (*Pnma*)	1.86 e	2.18 e	1.78 e	4.10 e	6.28	9.92 e

in the vicinity of E_F. Hence, only these states should be able to contribute to electron pair formation, favoring the view that the bonding mechanism in cubic GeTe is electron deficient, as in metavalent bonding. Yet, also the Ge s and Te s states are not fully occupied, so one might argue that they could also partially contribute to bond formation. Employing more advanced tools to characterize the bonds formed could provide further details.

The concept of the bond order can be put on a rigorous quantum mechanical basis, as shown by Wiberg and Mayer for molecules.[54,55] This concept can be extended to solids, as recently done by Dronskowski and co-workers.[56] The new quantity and the corresponding integrated version are called crystal orbital bond index (COBI) and ICOBI, respectively. Calculating the bond order for the three different phases of GeTe shows pronounced changes, both concerning the bond order, but also the effective coordination number (ECoN), which is introduced and discussed in more detail in the Supporting Information.[57]

The analysis of the bond order for the cubic phase in **Table 3** is close to 0.4, which corresponds to a sharing of 0.8 electrons. This is in reasonable agreement with metavalent bonding where two atoms are held together by a single electron (half an electron pair), but incompatible with hypervalence. Yet, one can wonder if quantum chemistry provides further tools to quantify chemical bonding.

3. Quantum-Chemical Bonding Descriptors to Differentiate and Quantify Different Bonding Mechanisms

In the last about 30 years, significant progress has been accomplished in the quantification of chemical bond properties in solids. These advances became possible with the development of the quantum theory of atoms in molecules (QTAIM) and its later application to solids. Within this framework, a basin Ω is assigned to each atom in a molecule or solid. Its boundaries are defined by surfaces that are not crossed by any gradient vectors of the electron density, hence called zero-flux surfaces. These so-called Bader basins are also often denoted as quantum domains, because their energy may be unambiguously defined as for the total system.[58] In order to analyze chemical bonds, we employ two different quantities for these domains. First, the net electronic charge of an atom, *Q*, is computed by integrating the one-electron density $\rho(\vec{r}_1)$ over its domain Ω and comparing it to the free reference atom. Doing so allows assessing the total positive or negative electron transfer (TET) to the domain surrounding, which is expected to be large in ionic solids but often small otherwise. Second, the DI for a pair of domains $\delta(\Omega, \Omega')$ is computed, which yields the number of electron pairs exchanged or shared between the corresponding domains Ω and Ω′. It is defined as

$$\delta(\Omega,\Omega') = \int_{\Omega'}\int_{\Omega} \rho_{xc}(\vec{r}_1,\vec{r}_2)\,\mathrm{d}\vec{r}_1\mathrm{d}\vec{r}_2 = \int_{\Omega'}\int_{\Omega} \left[\rho(\vec{r}_1)\rho(\vec{r}_2) - 2\rho_2(\vec{r}_1,\vec{r}_2)\right]\mathrm{d}\vec{r}_1\mathrm{d}\vec{r}_2 \quad (1)$$

where $\rho_{xc}(\vec{r}_1,\vec{r}_2)$ is the exchange-correlation density and $\rho_2(\vec{r}_1,\vec{r}_2)$ is the two-electron density or pair density. The former describes all nonclassical correlation effects influencing the probability distribution of two electrons, i.e., the Pauli exclusion principle (Fermi correlation) and Coulomb correlation, as it expresses the deviation of the pair density from the pure classical product of two independent densities. With an adequate normalization, the pair density is the probability to find one electron at $\vec{r}_1$ and another electron at $\vec{r}_2$, regardless of the position of the remaining ones. Thus, $\delta(\Omega,\Omega')$ provides a physical measure of a property that classical models associate with covalency, and it is amenable to comparison with formal bond orders. A full pair of electrons shared between neighboring atoms would correspond to the Lewis picture of a single covalent bond, i.e., a bond order of one.

In Kohn–Sham density functional theory (KS-DFT), the evaluation of the DI is not straightforward, since the pair density cannot be rigorously defined within this framework, since all kinds of correlation effects are implicitly already contained in the ideal DFT one-electron density. The pair density is therefore evaluated using a Hartree–Fock (HF)-like expression for the KS wavefunctions. Using the HF expression leads to the evaluation of the so-called domain overlap matrix (DOM), given by

$$S_{ij}(\Omega) = \int_{\Omega} \phi_i^*(\vec{r})\,\phi_j(\vec{r})\,\mathrm{d}\vec{r} \quad (2)$$

Table 3. ICOBI and average ECoN values calculated for three different phases of GeTe. The number of electrons forming bonds is obtained from the product of twice the bonder order (ICOBI) and the effective coordination number (ECoN). The definitions of ICOBI and ECoN are taken from refs. [56] and [57], respectively. The LOBSTER program package was used to calculate ICOBI.[35]

Phase	ICOBI	ECoN	Electrons forming bonds
Cubic (*Fm3m*)	0.39474	6.0	4.74
Rhombohedral (*R3m*)	0.63593	4.8	6.10
Orthorhombic (*Pnma*)	0.75535	3.4	5.14

where $\phi_i(\vec{r})$ and $\phi_j(\vec{r})$ are KS wavefunctions. The DI then takes the form

$$\delta(\Omega,\Omega') = 2\sum_{i,j}\Theta_i\Theta_j S_{ij}(\Omega)S_{ij}(\Omega') \tag{3}$$

with occupation numbers Θ_i and Θ_j of the corresponding states. Alternatively, the occupation numbers are defined as $\sqrt{\Theta_i}$. The first definition is the Ángyán and the second one is the Fulton formulation.[59,60] DOM analyses have been routinely performed for gas-phase molecules. Only very recently have such analyses been extended to the realm of plane-wave DFT and periodic systems.[31,32] Instead of the DI, which is the number of electron pairs shared between the basins, we will be focusing on the number of electrons shared between adjacent domains (ES = 2DI) as a bonding descriptor.[61] Also, the TET value is normalized by dividing it by the formal oxidation state of the corresponding atom. We name the normalized quantity ET.

It is desirable to decompose the electron pairs formed between adjacent atoms into contributing localized orbitals. This task can be accomplished with the help of the so-called domain averaged Fermi hole (DAFH). The DAFH was first introduced by Robert Ponec and has its origins in the Fermi hole introduced by Wigner to investigate coupling of same spin electrons in solids.[62,63] Despite its name, the Fermi hole contains in principle both Coulomb and Fermi correlation. The Fermi hole is defined as

$$\rho^{\text{hole}}(\vec{r}_2|\vec{r}_1) = \rho(\vec{r}_2) - 2\underbrace{\frac{\rho_2(\vec{r}_1,\vec{r}_2)}{\rho(\vec{r}_1)}}_{\rho^{\text{cond}}(\vec{r}_2|\vec{r}_1)} = \frac{\rho_{xc}(\vec{r}_1,\vec{r}_2)}{\rho(\vec{r}_1)} \tag{4}$$

where $\rho^{\text{cond}}(\vec{r}_2|\vec{r}_1)$ is the conditional probability density to find one electron at $\vec{r}_2$ given that another electron, called reference electron, is at position $\vec{r}_1$. It therefore describes the deviation from the one-electron density in the presence of the reference electron. The subsequent integration of the Fermi hole is motivated by the fact that, due to the Heisenberg uncertainty principle, it is unphysical to fix the reference electron at a specific point in space. Furthermore, it has been shown by Luken that $\rho^{\text{hole}}(\vec{r}_2|\vec{r}_1)$ is relatively localized in certain regions, e.g., around nuclei. Therefore, it makes sense to integrate the reference electron's position over an appropriate region Ω (domain-averaging).[64] In addition to that, this new integrated version of the Fermi hole is customarily normalized to the number of electrons in the basin N_Ω (charge-weighting)

$$G^{\Omega}(\vec{r}_2) = N_\Omega\int_{\Omega}\rho^{\text{hole}}(\vec{r}_2\,|\,\vec{r}_1)\mathrm{d}\vec{r}_1 = \int_{\Omega}\rho_{xc}(\vec{r}_1,\vec{r}_2)\,\mathrm{d}\vec{r}_1 \tag{5}$$

The quantity $G^{\Omega}(\vec{r}_2)$ is called DAFH. Its relation to the DI can directly be seen by comparing it to Equation (1). Whereas in DI all positional degrees of freedom have been integrated out, the DAFH still has a positional dependence. Diagonalizing the matrix representation of the DAFH in the basis of KS orbitals yields eigenvalues (occupation numbers) and eigenvectors (DAFH orbitals) that are then subjected to the so-called isopycnic transformation. The isopycnic transformation maximally localizes the DAFH orbitals while preserving the DAFH density. However, after the transformation the DAFH orbitals is no longer orthogonal. Fermi holes associated with a region Ω are predominantly localized in Ω. Hence, the occupation numbers and DAFH orbitals provide information about the structure of such regions. If a single atom domain is analyzed, the hole yields information about the valence state of the atom in the molecule or solid. If the domain includes several atomic regions, the hole reveals both the electron pairs (chemical bonds, lone pairs, etc.) that remain intact in that fragment and the broken or dangling valences formed by forcing the fragment to isolate itself from the rest of the system. Structural information is evinced both from the occupation numbers and through the visual inspection of the corresponding DAFH orbitals. It is then possible to calculate the contribution to the number of electrons shared in a bond between two atoms from DAFH orbitals of their joint two-atom domain, relating ES and associated DAFH orbitals.

It is well-known that DFT exhibits some inherent shortcomings, which might affect the calculated values of ES and ET. The generalized-gradient-approximation Perdew–Burke–Ernzerhof functionals used generally yield reasonable results, but are still an approximation of the true exchange-correlation functional. This results in an underestimation of the bandgap, e.g., The use of DFT also calls for an approximation in the determination of the DIs, since a pair density does not exist in DFT. As mentioned before, we are forced to use an HF-like expression for the pair density and for determining the DIs values. Furthermore, the basins used for real-space integration were obtained using the Bader method, while other definitions exist as well. However, for the many compounds we have calculated so far, we have observed that the chemical expectations are reproduced, including archetypical compounds like diamond, NaCl, and Al. Furthermore, we have used different codes (Quantum Espresso in conjunction with Critic2 and Abinit with DGRID) to test the consistency of the results. The difference in ES and ET was found to be smaller than the markers used in **Figure 3**.[60] Hence, we are confident that the values are a good representation of the actual chemistry at hand. Concerning spin–orbit (relevant in, e.g., PbTe) and van-der-Waals corrections (relevant in, e.g., γ-GeTe), we found that the ES and ET values did not change significantly.[6,65] Therefore, these corrections are not included in the calculations presented here.

We will now take GeTe as an example to calculate DI, ES, ET, and the DAFH orbitals with the help of the software packages DGrid and Critic2.[32,33] With these quantum mechanical tools, the chemical bonding mechanism employed in GeTe can be characterized. The ES and ET values for cubic (*Fm3m*) and trigonal (*R3m*) GeTe are shown in **Table 4**. In contrast to the large ET values in NaCl, the small values of ET in GeTe suggest that the bond between Ge and Te is not predominantly ionic. In addition to that, ES is just 0.88 for both, Ge and Te in the cubic and 1.3 in the shorter bond of the rhombohedral compound. For a covalent bond, one would expect one electron pair, i.e., two shared electrons as it is the case for diamond (see Table 4). Instead, we find less than 1 shared electron, i.e., less than half of an electron pair for cubic GeTe. This is compatible

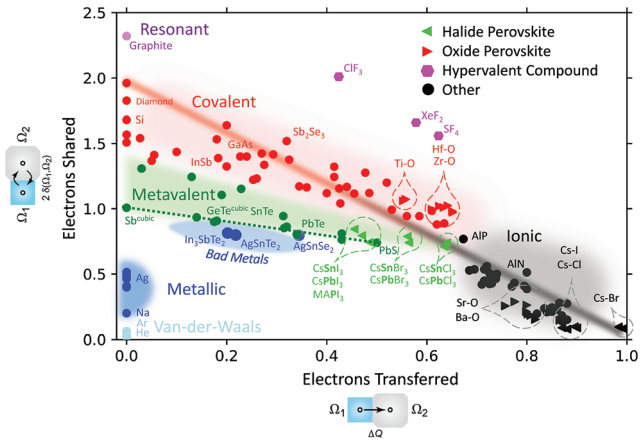

Figure 3. 2D map classifying chemical bonding in solids. The map is spanned by the number of electrons shared between adjacent atoms and the electron transfer renormalized by the formal oxidation state. Different colors characterize different material properties and have been related to different types of bonds. Reproduced with permission.[61] Copyright 2019, RWTH Aachen University, published by Wiley-VCH/Reproduced with permission.[66] Copyright 2018, RWTH Aachen University, published by Wiley-VCH. Filled and open symbols represent thermodynamically stable and metastable phases. Triangles pointing left are utilized for halide perovskites, and those pointing right for oxide perovskites. For these compounds, the element in bold characterizes the bond considered. Hypervalent compounds (3c–4e) are denoted by magenta-colored hexagons. The red–black line describes the transition from ideal covalent bonds to perfect ionic bonds. The dashed green line indicates metavalently bonded solids with perfect octahedral arrangement like cubic Sb, $AgSbTe_2$, and PbS, while distorted octahedrally coordinated structures are situated above it, characterized by a larger number of electrons shared. Map revised under the terms of the CC-BY Creativwe Commons Attribution 4.0 International license (https://creativecommons.org/licenses/by/4.0).[67] Copyright 2021, The Authors, published by Springer Nature.

with the calculated ICOBI values of about 0.4, shown in Section 2 (Table 3). Hence, we conclude that the bond in this case is neither ionic nor covalent. Furthermore, cubic GeTe does not employ a metallic bond, since it opens up a bandgap due to the small charge transfer, i.e., small ET.

With the help of the DAFH orbitals, the contribution of orbitals to the formation of bonds can be determined. In **Table 5**, the occupation and localization of certain DAFH orbitals, as well as their contribution to the DI are shown. We can see that the 3d orbitals of Ge do not contribute at all to the DI, as their localization within the bond partner basin is negligibly small. This also holds for the 4d orbitals of Te (not shown). Also, the 4s orbitals of Ge hardly contribute. This can be seen from the small localization in the partner basin as well as the modest contribution to the DI. The same is true for the 5s orbital of Te. This contrasts with the "hypervalent 3c–4e," the "10 electron solids," and the "lone pair involved" bonding schemes discussed in Section 2, which all assume that the Ge 4s orbital (and possibly even the Te 5s orbital) plays an important role in bond formation. Instead, Table 5 reveals that the three 4p orbitals of Ge and Te provide the major contribution to the DI, with 0.28 and 0.30 electron pairs each, respectively. From this analysis, one can thus conclude that the dominant bonding contribution comes from the overlap of the p orbitals, where about one electron is shared between adjacent atoms. Hence, the four different approaches to characterize bonding in GeTe provide a very coherent view. From the analysis of the DoS, one can derive that the s orbitals of Ge and Te are almost completely filled, and hence cannot contribute to bonding (in analogy with the fact that He does not form a stable He_2 molecule). Instead, the p orbitals of Ge and Te govern the bonding. A total number of six p electrons are hence available for the six σ-bonds formed between adjacent atoms. Since there is little electron transfer between adjacent atoms, most of these electrons can be shared between adjacent atoms. This leads to an ES of slightly less than 1, i.e., slightly less than half an electron pair, in line with the bond order of about 0.4 determined from the ICOBI. Finally, the DAFH analysis confirms that the bond formation is governed by p orbital overlap. The bonding configuration described above differs significantly from covalent, ionic, or metallic bonding mechanisms.

Table 4. ES and ET values for cubic (*Fm3m*), the shorter bond of trigonal (*R3m*) phase of GeTe (β-GeTe and α-GeTe, respectively), NaCl, and diamond calculated with DGrid based on DFT performed with Quantum Espresso.

Cubic GeTe			Rhombohedral GeTe		NaCl		Diamond
	Ge	Te	Ge	Te	Na	Cl	C
ET	–0.18	0.18	–0.18	0.18	–0.87	0.87	0
ES	0.88	0.88	1.3	1.3	0.128	0.128	1.8

Table 5. Localization within bond partner basin calculated from a DAFH orbital analysis for cubic GeTe using the atomic arrangement of the materials project data file (mp_2612) and subsequent structural relaxation.[13] The data in the table describe the contribution of each single DAFH orbital. For the p orbitals, there are significant contributions to two opposite neighbors with identical localization. The DAFH orbitals of rhombohedral and orthorhombic GeTe are provided in the Supporting Information.

DAFH orbitals	Occupation, e	Localization within native basin	Localization within bond partner basin	DI contribution
Ge				
4p (3x)	0.51	27.5%	27.32% (2x)	0.28 (Ge–Te)
4s	1.74	87.7%	1.7% (6x)	0.06
3d (5x)	2	>99.9%	–	–
Te				
5p (3x)	1.31	66%	11.4% (2x)	0.299 (Te–Ge)
5s	1.88	94.3%	0.8% (6x)	0.029 (Te–Ge)

4. Quantum-Chemical Bonding Descriptors to Map Different Bonding Mechanisms

In the preceding section, different quantum chemical bonding descriptors have been introduced. These descriptors enable a comparison of different solids. One key goal of this approach has already been depicted in Figure 1. A precise characterization of chemical bonding could be employed to understand, explain, and design the properties of advanced functional materials. In this section, the mandatory first step for this procedure will be explored. We will check, if modern quantum chemical bonding descriptors will help to distinguish different bonding mechanisms.

To this end, a map is displayed in Figure 3 which is spanned by the two different quantum chemical bonding descriptors introduced in the previous section. The electron transfer between adjacent atoms is utilized to create the *x*-axis. To account for the different oxidation states of O in MgO and Cl in NaCl, the total number of electrons transferred is divided by the formal oxidation state (nominal ionic charge). This makes it easier to compare the degree of ionicity in, e.g., alkali halides and alkaline earth oxides. The *y*-axis is spanned by the number of electrons shared between adjacent atoms. The number of electrons shared between these atoms is twice the number of electron pairs formed between adjacent atoms.

The map in Figure 3 nicely separates solids with predominantly ionic bonds such as NaCl, from materials which employ metallic bonding, such as elemental Na and covalent bonds as found in Si or GaAs. Ionic compounds such as NaCl, MgO, or LiF are characterized by a significant amount of electron transfer. At the same time, there is very limited electron pair formation between adjacent Na and Cl ions in NaCl. This is very different from the scenario encountered in Si or Ge, where there is no charge transfer between adjacent atoms, but about one electron pair is shared between these two atoms, i.e., almost two electrons are shared. This corresponds to a classical covalent bond between two atoms, a 2 center–2 electron bond (2c–2e bond). This bonding concept was introduced by Gilbert Lewis in 1916, and shortly afterward termed "covalent bond" by Irvin Langmuir.[68,69] In metals like Na or Mg, finally, there are too few electrons available to form covalent bonds due to the large number of nearest neighbors. These "electron-deficient" solids thus cannot form an electron pair, i.e., a 2c–2e bond, between adjacent atoms. These metals thus share a smaller number of electrons.

The map in Figure 3 has a number of advantages compared to previous generations of maps, such as the first generation of maps developed around 1940 by van Arkel and Ketelaar, depicted in the Supporting Information, or the maps developed around 1970 by van Vechten, Philips, and Littlewood (see Supporting Information).[70–77] These previous generations of maps were based on empirical atomic quantities such as the average electronegativity of the elements involved, as well as the difference in electronegativity of these elements (van Arkel, Ketelar). In the second generation of maps (van Vechten, Philips), the ionicity as well as the hybridization, two quantities determined from the orbital radii of the valence electrons derived from pseudo-potentials were utilized. Since all of these quantities are atomic quantities, different phases of the same compound had the same quantum-chemical bonding descriptors and hence the same position in these first two generations of maps. Hence, it was impossible to distinguish graphite from diamond, even though these two carbon allotropes have very different properties.

The map depicted in Figure 3 clearly separates diamond, where ordinary covalent bonds prevail, from graphite, where adjacent atoms form an ordinary covalent bond, a 2c–2e σ-bond and a second bond, a π-bond, where adjacent atoms share half an electron pair (one electron). Hence, in graphite, adjacent carbon atoms share three electrons (2c–3e bond), rather different from the bonding pattern in diamond. Yet, this map has further advantages. It enables, e.g., a quantitative description of the transition from covalent to metallic or ionic bonding within the framework of sharing and transferring electrons. In most textbooks about solids, on the contrary, the different bonding types are explained by concepts which do not enable a discussion of transitions between bonding mechanisms. The characterization of ionic bonding, e.g., usually focuses on the Coulomb energy between the ions (the Madelung energy). Covalent bonding, on the contrary, is attributed to orbital overlap between adjacent atoms.[78] Finally, metallic bonding is frequently discussed in terms of the energetic benefits of electron delocalization by a reduction of kinetic energy. Hence, it is very difficult to quantify transitions between the different bonding mechanisms. The map in Figure 3 instead explains the transitions between these bonding mechanisms by changes in the number of electrons transferred and shared between adjacent atoms. Hence, these two quantities are apparently good quantum-chemical bonding descriptors.

Yet, the map contains another surprise. Between covalent and metallic bonding, there is a region where compounds like GeTe, Sb_2Te_3, Bi_2Se_3, PbTe, and PbSe are found. These materials are characterized by a distinct property portfolio, including an effective coordination number which is larger than expected for ordinary covalent bonding, an electrical conductivity at room temperature which approaches values typically observed for metals, large Born effective charges, a measure of chemical bond polarizability, rather soft bonds as evidenced by high values of the Grüneisen parameter for transverse optical modes, and a large electronic polarizability, as can be seen from the high values of the optical dielectric constant.[57,66] The map indicates that the bonding mechanisms of metallic, ionic, covalent, and metavalent bonding are distinct bonding mechanisms. We will later substantiate this statement, e.g., by emphasizing the unique property portfolio that accompanies materials which possess these bonding mechanisms.

However, it is also tempting to ponder if the differences between these bonding mechanisms can be visualized to explain their dissimilarities. After all, a devil's advocate might argue that ionic, metallic, and covalent bonds are simply idealistic limiting cases that are not particularly relevant to understand, explain, and predict material properties. Hence, we are looking for a quantity which relates the concept of chemical bonding to an orbital view which has thrived over the last 100 years. The DAFH can help build this bridge. In particular, DAFH orbitals yield a visual and chemically clear representation of the bonding in position space between the domain Ω and its neighborhood, capable to recover many chemical

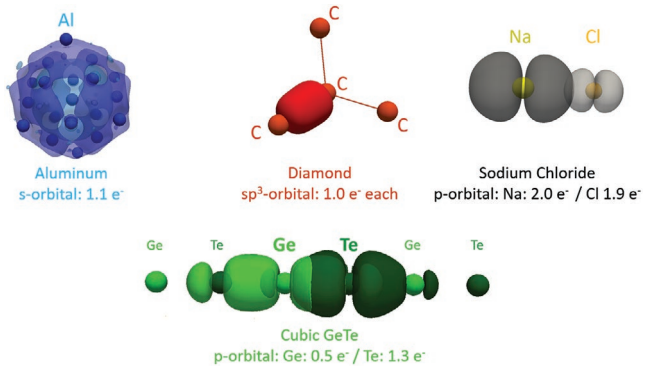

Figure 4. Representative DAFH orbital shapes for different bonding patterns focusing on the joint contribution of adjacent orbitals (except for Al). Metallic bonding—Al: represented by the outermost s orbital, which extends to neighbors from the first and second coordination shells. Covalent bonding—diamond: orbital shapes localize mostly in-between two bonding atoms. Ionic bonding—NaCl: orbital shapes do not deviate significantly from the corresponding shapes of atomic orbitals expected in isolated atoms. Metavalent bonding—GeTe: p-like orbitals localize most between the native atom and two closest neighbors on opposite sites. The numbers below the figures specify, how many electrons are in the corresponding orbital. For Al, 1.1 e is located in the s orbital, for diamond, each of the 2 adjacent atoms contributes with 1 e to an sp^3 hybrid, forming an electron pair. In NaCl, a p orbital each is filled for Na (2p) and Cl (3p), with very limited overlap between them. Finally, in GeTe, Ge contributes 0.5 e, while Te deploys 1.3 e, in total 1.8. Since these electrons are shared with 2 neighbors, only about ½ electron pairs (about 1 e) is available for bond formation between adjacent atoms. Orbital isosurfaces are set to 0.03 for Na (in NaCl) and Ge in GeTe, –0.03 for Cl (in NaCl) and Te in GeTe, 0.2 in diamond and ±0.005 in Al. The DAFH orbital tables for Al, diamond, and NaCl can be found in the Supporting Information.

concepts originally appeared in the orbital-based approach.[62,63] The domain population as well as the value of delocalization indices can be decomposed into the sum of contributions from these orbitals. Usually, only very few DAFH orbitals contribute significantly. This is very advantageous to describe solids, which frequently require numerous delocalized Bloch states for an adequate description.

In **Figure 4**, relevant DAFH orbitals for four different bonding mechanisms are depicted, representing typical cases of metallic, covalent, ionic, and metavalent bonding. Obvious differences for the corresponding DAFH orbitals of the outer valence shells are visible. For Al, the DAFH orbital of the outermost s electron extends over several neighbors, characteristic for the delocalized nature of metallic bonding. In covalent bonding, as depicted for diamond, each atom contributes about one electron to its nearest neighbor, forming an electron pair, as already suggested by Lewis about 100 years ago. For the ionic bonds formed in NaCl, the outermost orbitals of Na and Cl are almost completely filled, with 2.0 and 1.9 electrons, respectively, due the electron transfer between Na and Cl. Yet, the overlap of these p orbitals is marginal, as can be seen in Figure 4. Interestingly, metavalent bonding as realized in cubic GeTe, e.g., differs significantly from all other three bonding types depicted. For Ge and Te, 0.5 and 1.3 p electrons are employed, respectively. Hence, in total about 1.8 p electrons form bonds between adjacent atoms. However, these electrons are distributed over a chain of three atoms, so that a kind of 3c–2e bond is formed. Between two adjacent atoms, only about one p electron, or half an electron pair is located, very different from both metallic and covalent bonding. The DAFH orbitals depicted in Figure 4 hence help to visualize the differences between metallic, ionic, and covalent bonding and confirm the distinct nature of metavalent bonding.

To stress the contribution of different orbitals, **Figure 5** focuses on single orbitals and their extent. This helps to see more clearly how small the orbital overlap is for ionic compounds. The analysis of DAFH orbitals also helps to understand the nature of the transition between metavalent and covalent bonding. This transition has already been addressed in terms of a chemical bonding analysis by Raty and Wuttig.[79]

As can be seen in **Figure 6**, for the cubic phase, i.e., for vanishing Peierls distortion, a pronounced DAFH orbital of p electrons with equal value is formed with two equally spaced neighboring atoms. Upon increasing Peierls distortion, the DAFH orbital for the shorter bond significantly increases. This makes this bond more covalent, and a concomitant decrease of the DAFH orbital for the longer bond is observed. The average of both values, however, is practically constant, reflecting the fact that the p orbitals are aligned along a chain of atoms and are either located between the center atom and the right or the left neighbor. No significant changes are observed for the valence s states of Ge ($4s^2$) and Te ($5s^2$). This indicates that these s states, sometimes denoted as lone pair states, do not play any prominent role for bonding in monochalcogenides such as GeTe, SnTe, PbTe, or PbSe. They should rather be considered as semicore states. The changes in orbital overlap of the p states also lead to significant changes of material properties upon increasing Peierls distortion. This is depicted in **Figure 7**b), where the maximum value of the imaginary part of the dielectric function is shown, which governs the absorption of photons. It is remarkable that the pronounced change in optical properties (and other band structure-related features) can be realized upon small changes of energy. This is another characteristic of metavalent solids. In the next section, the relationship between chemical bond descriptors and a number of different material properties will be discussed in more detail.

5. Quantum-Chemical Bonding Descriptors to Explain and Predict Material Properties

In the previous section, recent advances in quantum chemistry have been discussed, which provide a metric to quantify chemical bonding. The two quantum chemical bonding descriptors introduced can be employed to describe transitions between bonding mechanisms, such as the transition between covalent and ionic bonding, or the transition between covalent and metallic bonding. The ability to describe these transitions as changes of ES and ET demonstrates that these two quantities are good quantum-chemical bonding descriptors.

Yet, this review strives for a more ambitious goal. We hope to design advanced functional materials through a detailed understanding of bonding in solids. The question thus arises if ES and ET possibly will also be good property predictors? In the following, we will focus on three different applications: photovoltaics, PCMs, and thermoelectrics. For all of these

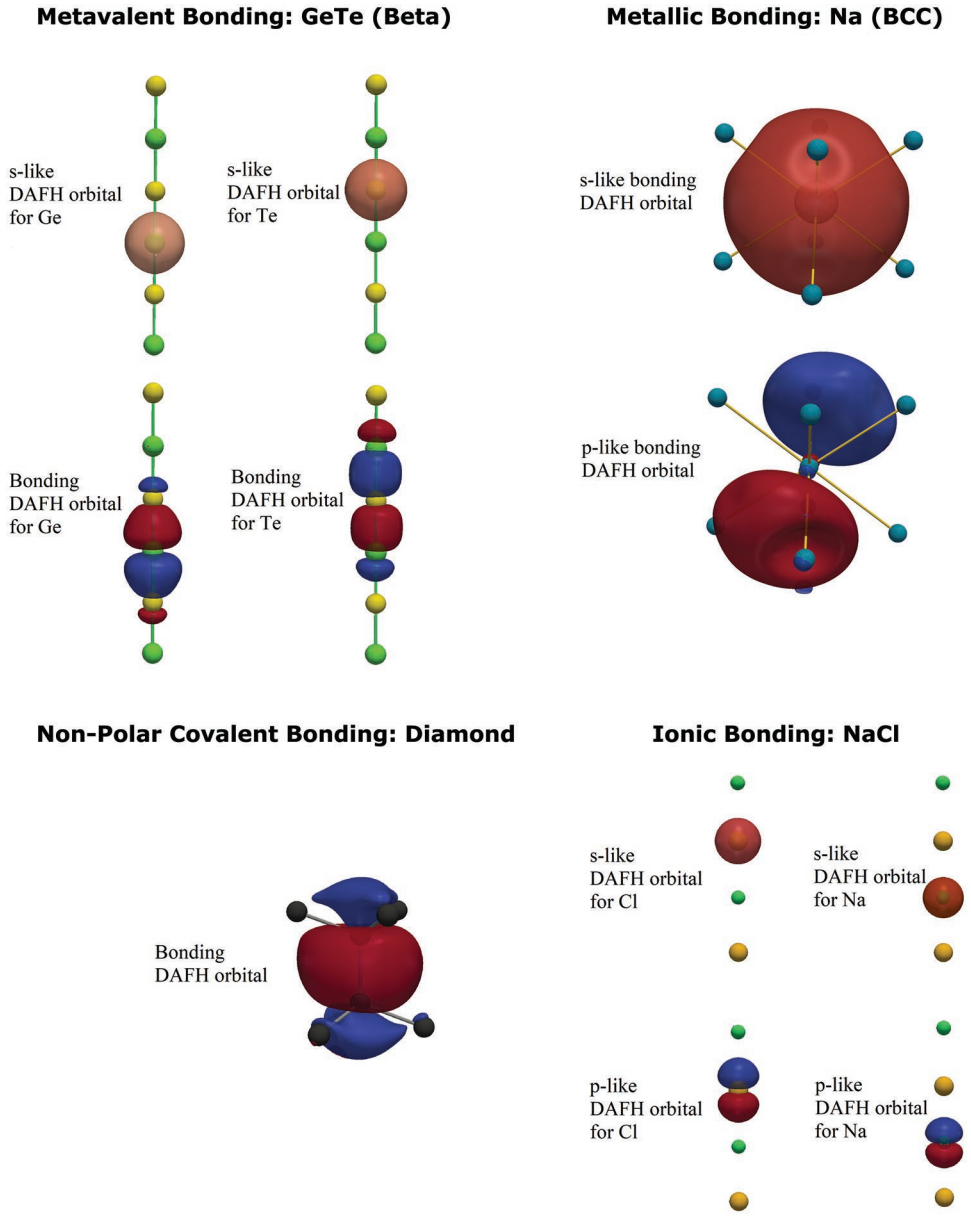

Figure 5. DAFH orbitals associated with the outer valence shells are considered only, i.e., 2s, 2p states for C; 3s, 3p states for Al, Na, and Cl; 4s, 4p states for Ge; and 5s, 5p states for Te. For diamond, only one DAFH orbital per atom is depicted since s and p orbitals are mixed to form four equivalent bonds. Orbital isosurface is set to |0.025| for all compounds. The DAFH orbital tables for Al, diamond, and NaCl can be found in the Supporting Information.

applications, chalcogenides and related p-bonded solids are intensely studied. Hence, we will focus on these materials here. Chalcogenides such as GeTe, PbTe, PbSe, Sb_2Te_3, and Bi_2Se_3 were presented in the last section as metavalently bonded materials. In this section, the unconventional properties that are characteristic for these solids will be related to the prevalent bonding mechanism. First, examples of the correlation of physical properties and chemical bonding are shown. Then, the reasons for the close relationship between material design and chemical bonding are addressed. Finally, the causal relationship is used to develop design rules for specific application areas.

Figure 7 visualizes the step from a 2D map, which offers a quantitative description of chemical bonding, to a 3D map, which relates chemical bonding descriptors (ES, ET) and property trends. The finding that these properties change systematically upon changing ES and ET demonstrates their ability to predict properties. Increasing ES for metavalent solids, e.g., increases the Peierls distortion, which leads to a concomitant increase of the bandgap, as well as a decrease in electrical conductivity. These trends for metavalent solids can be explained by the unique bonding situation in metavalent solids as will be shown below.

Figure 7b shows systematic changes for the maximum photon absorption, i.e., $\varepsilon_2(\omega)_{max}$ for these monochalcogenides as a function of ES and ET. This figure reveals a remarkably clear trend for $\varepsilon_2(\omega)_{max}$. This quantity decreases with increasing

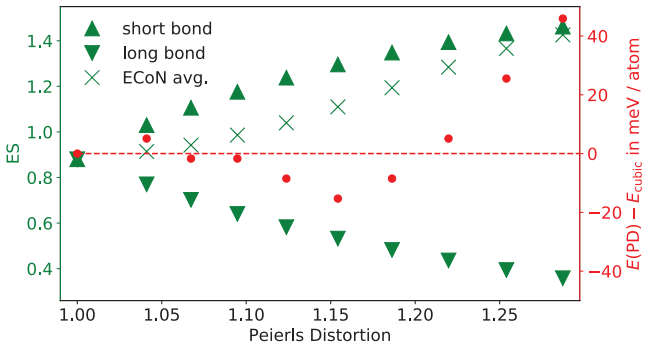

Figure 6. Changes in bonding of GeTe upon increasing Peierls distortion. Moving from the simple cubic structure of GeTe to a rhombohedral phase with increasing Peierls distortion leads to significant changes in the number of electrons shared (ES) for short and long bonds (green triangles pointing up and down) and their ECoN-average (green cross), while the energy of these phases only shows modest changes.

ET as well as ES increasing away from the green dotted line shown in Figure 7, i.e., upon increasing Peierls distortion. These clear trends can be explained thoroughly, as discussed in the next sections. Figure 7c finally shows systematic changes for the chemical bond polarizability, i.e., the Born effective charge Z^*. Again, this figure reveals clear trends. Z^* decreases, on average, with increasing ET along the dashed green line, and decreases systematically upon increasing ES away from this line. Please note that in Figure 6c we depict the elevated Born effective charge Z^*_+, which is obtained upon dividing Z^* by the formal oxidation state. This facilitates the comparison of different materials. We have not found another set of bonding descriptors which can explain property trends so well. This consolidates the conclusion that ES and ET are excellent property predictors for the chalcogenides discussed here. They are apparently the "natural" variables to describe systematic trends for the properties of metavalent solids.

In the next sections, arguments will be sketched, why ES and ET are such good property predictors. Many relevant properties

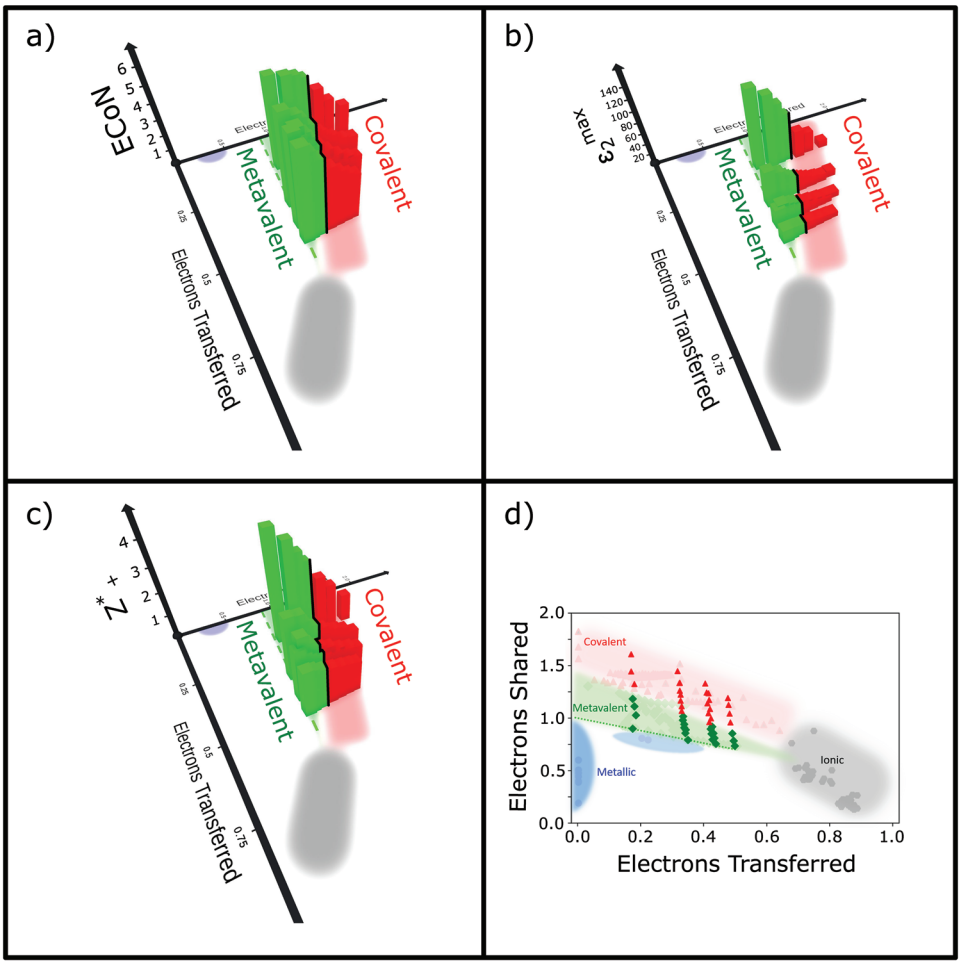

Figure 7. Various properties plotted against electrons shared and electrons transferred for different monochalcogenides. The (stable) cubic systems are located along the dashed green line (ECoN of about 6). With increasing distortion, ECoN decreases, while ES increases. a) Effective coordination number (ECoN), b) maximum of the imaginary part of the dielectric function $\varepsilon_2(\omega)_{max}$, c) elevated Born effective charge Z^*_+, d) 2D version of the ES/ET map with the monochalcogenides highlighted. Reproduced under the terms of the CC-BY Creative Commons Attribution 4.0 International license (https://creativecommons.org/licenses/by/4.0).[80] Copyright 2022, The Authors, published by American Assocaition for the Advancement of Science.

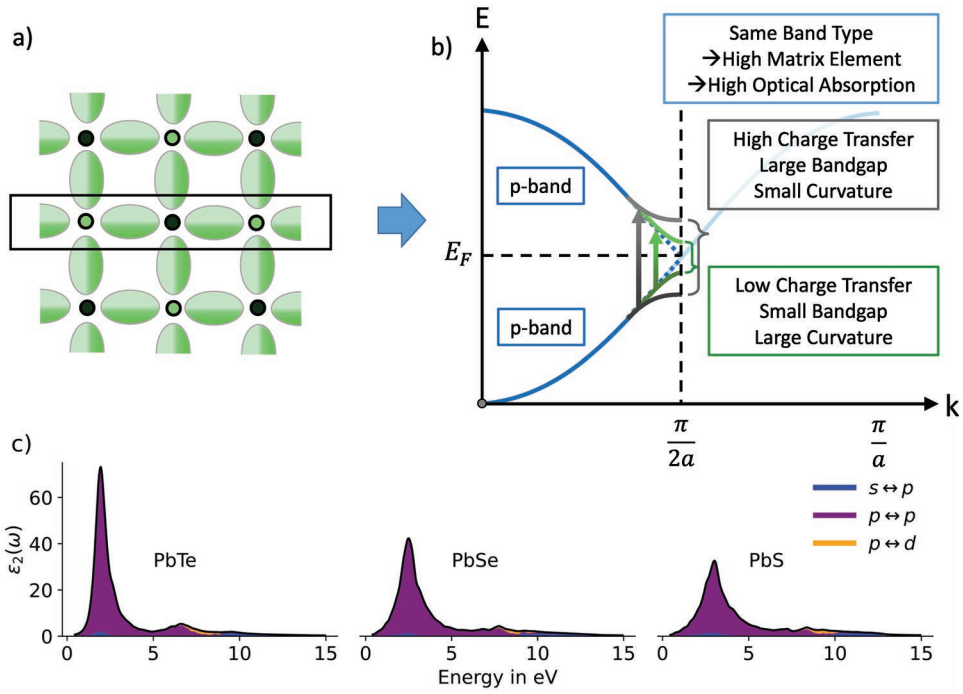

Figure 8. a) Bond formation and b) resulting band structure in PbTe. Atomic orbitals of Pb and Te responsible for bond formation in the solid are depicted on the left-hand side. The atomic arrangement in the (001) plane is shown, where small electron transfer and the formation of σ-bonds between adjacent atoms are responsible for bond formation. The σ-bonds are occupied by about half an electron pair (ES ≈ 1), resulting in an almost metallic band (blue curves on the right side). However, the small charge transfer results in a small bandgap (ET = 0.34). c) Resulting dielectric function for PbTe, PbSe, and PbS. The p–p transition dominates, while s–p and p–d transitions only play a minor role. Reproduced with permission.[81] Copyright 2020, The Authors, published by Wiley-VCH.

of solids such as the bandgap, the optical absorption, or the effective masses of charge carriers are closely related to the electronic band structure of the solid. Therefore, we will start by relating the bonding scheme in chalcogenides and similar compounds with the resulting band structure. Most chalcogenides discussed here are characterized by a perfect octahedral or octahedral-like atomic arrangement. This is schematically shown in **Figure 8**a for the case of PbTe. The chemical bond between adjacent atoms is predominantly formed by overlapping p orbitals which form a σ-bond. Yet, there are only six electrons in this bond, for all six neighbors. Without any charge transfer between adjacent atoms, i.e., for a solid-like cubic Sb, a metallic phase would be created at reasonable interatomic spacing. In PbTe, the charge transfer from Pb to Te opens as small bandgap. The valence band is predominantly occupied by Te p states, while the conduction band consists mainly of Pb p states. This can be seen from an analysis of the integrated DoS, which determines that there are 4.3 p states of Te in the valence band, while there are 4.1 p states of Pb in the conduction band.

Figure 8 emphasizes the close relationship between chemical bonding, band structure, and optical properties. The overlap of adjacent p orbitals of Pb and Te atoms dominates the valence and conduction band. The larger the orbital overlap, the smaller the corresponding bandgap. This leads to a large curvature of the bands in the vicinity of the zone boundary (L-point of the Brillouin zone). Interesting trends are observed for the optical properties of the Pb monochalcogenides. Going from PbTe to PbSe and PbS, a decrease in the maximum of $\varepsilon_2(\omega)$ is observed, which moves to higher energies (Figure 8c). This systematic trend deserves an explanation. The energy dependence of $\varepsilon_2(\omega)$ can be explained by first-order perturbation theory, summarized by Fermi's golden rule.[82,83] Using this rule, the dielectric function in a single particle picture is given by

$$\varepsilon_2(\omega) \sim \frac{1}{\omega^2} \sum_{cvk} \left| \langle c | \nabla_k | v \rangle \right|^2 \delta\left(\omega - (E_c - E_v)\right) \tag{6}$$

where $|v\rangle$ and $|c\rangle$ are valence and conduction band states with energies E_v and E_c. $\varepsilon_2(\omega)$ is governed by the joint DoS $\approx \sum_{cvk} \delta(\omega - (E_c - E_v))$ stemming from the valence and conduction band energies, and by the matrix element $\langle f|\nabla k|i\rangle$ for the transition between these states. The orbital decomposition shows that p–p (σ–σ^*) transitions govern the dielectric function. In **Figure 9**, the dielectric function $\varepsilon_2(\omega)$ is decomposed into its two factors, the matrix element and the joint DoS. Interestingly, the joint DoS does not change its shape considerably, moving from PbTe to PbSe and PbS. It mainly shifts to higher energies due the increasing bandgap. The matrix element, however, decreases significantly along this line from PbTe to PbS. This can be attributed to a reduction in orbital overlap along this line, which is closely related with the increase of ET. ET is hence a property predictor!

We note in passing that such chalcogenides with rock salt structure have a favorable dispersion, where the valence band maximum and conduction band minimum are at the L point

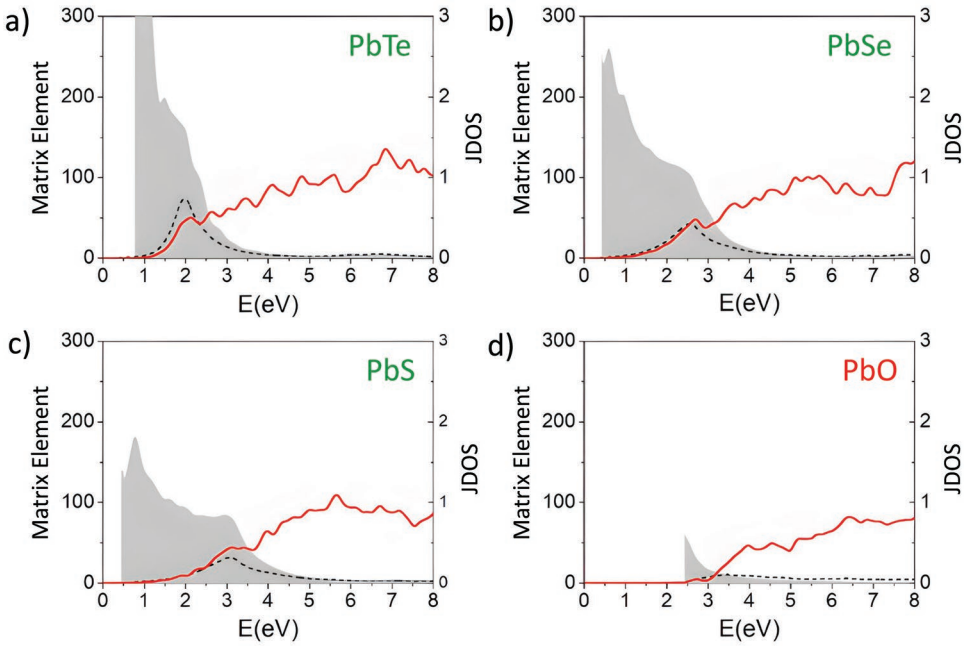

Figure 9. Matrix element (ME) and joint density of states contributing to the total imaginary part of the dielectric function $\varepsilon_2(\omega)$ in the energetic region of the electronic interband transitions shown in Figure 6. Left axis: matrix element (ME, gray area) and total $\varepsilon_2(\omega)$ (dashed line); right axis: joint density of states (red, DOS normalized per atom). When going from PbTe to PbO, the decrease in $\varepsilon_2{}^{max}$ and broadening of $\varepsilon_2(\omega)$ can be attributed to changes in the matrix element ME causing a change in the electronic interband transition rate. The reduced transition rate can be explained by a reduced orbital overlap between initial and final state. This reduction is related here to the increasing charge transfer, as described by ET.

and have a large degeneracy, which leads to a significantly higher DoS effective mass, which is ideal for thermoelectric applications.[84,85]

While several monochalcogenides have a simple rock salt structure, GeTe has a distorted rock salt structure.[86] It is hence important to understand the impact of this distortion on the properties of chalcogenides. This is demonstrated in **Figure 10**. Since the size of the Peierls distortion is closely related to ES (see Figure 6), and the Peierls distortion has a pronounced impact on the optical properties, ES has a pronounced impact on the optical properties. As can be seen from Figure 10, an increasing Peierls distortion has a strong impact on $\varepsilon_2(\omega)$, since the matrix element for the transition between the valence and conduction band decreases, due a decrease of the orbital overlap of the initial and final state upon increasing distortion.

While Figure 7 has shown that ES and ET are good property predictors, at least for the dielectric function $\varepsilon_2(\omega)$, Figures 9 and 10 explain this close relationship. As can be seen from Fermi's golden rule, the pronounced maximum seen for the chalcogenides presented in these figures is due to the impact of ES and ET on the orbital overlap, which governs the dielectric function. This explains why ES and ET are excellent property predictors for metavalent solids.

Now that this close relationship between chemical bonding and resulting material properties has been discussed and explained, it can be employed to tailor the properties of advanced functional materials. This will be done for three classes of materials: photovoltaic absorbers, PCMs, and thermoelectrics. The maximum of the dielectric function $\varepsilon_2(\omega)$ is very important for solar cell absorbers, e.g., since it describes the efficiency with which photons can create electron–hole pairs. The pronounced overlap of p orbitals of adjacent atoms explains why recently chalcogenides are being discussed as interesting materials for photovoltaic absorbers.[87–92] Instead of discussing this material class, we will focus on halide perovskites. First suggested for their favorable optical properties in 1999 by Mitzi, Snaith, and co-workers showed in 2012 and following that these halide perovskites can reach high efficiencies.[93,94] **Figure 11** reveals that the favorably strong optical absorption, which ensures a high efficiency of photon to electron–hole pair conversion is caused by the strong orbital overlap of Pb and I p states, which form a network of σ-bonds. These bonds resemble the metavalent bonding discussed for monochalcogenides above. This argument can be strengthened by a quantum-chemical bonding analysis which determines the number of electrons shared and transferred between adjacent atoms. The result of this analysis is depicted in Figure 3, which confirms the conclusion that the bonding in lead chalcogenides and halide perovskites closely resemble each other.[6] While the similarities in material properties had already been noted previously, Figure 3 reveals the similarity from a perspective of quantum-chemistry.

Figure 3 underlines the similarity between the bonding between lead chalcogenides and the B—X bond in halide perovskites (ABX_3, where X is a halogen atom). Figure 3 also helps to understand and predict property trends. Replacing the halogen atom iodine (I) by fluorine will increase the bandgap, but also reduce the efficiency of electron–hole creation upon photon absorption considerably. More importantly, the effective masses of electrons and holes will increase substantially with increasing bandgap, a relation discussed in the caption of Figure 10 for GeTe already.[6]

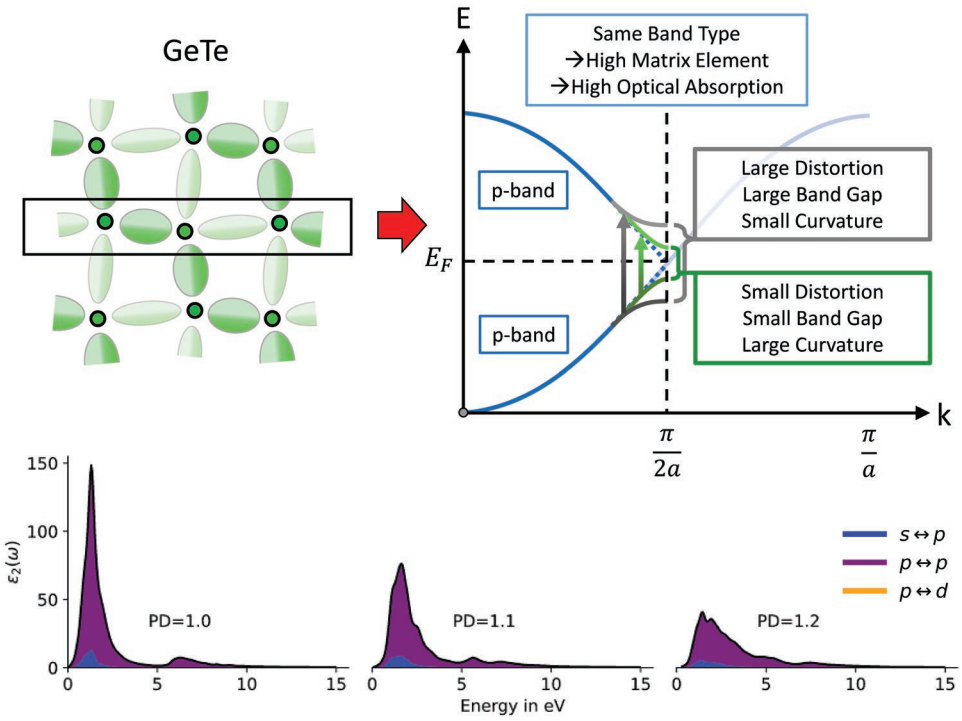

Figure 10. Illustration of the bond formation in GeTe and the resulting band structure: atomic orbitals of Ge and Te responsible for bond formation in GeTe are depicted on the left. σ-bonds are formed from p orbitals, which are occupied by about half an electron pair (ES ≈ 1), resulting in a metallic band (blue curves on the right side of the figure). However, moderate charge transfer and significant electron sharing (moderate Peierls distortion) result in a small bandgap. Increasing the Peierls distortion leads to a further opening of the bandgap, a smaller curvature and hence a larger effective mass. This also has pronounced consequences on the imaginary part of the dielectric function, i.e., $\varepsilon_2(\omega)$. This is shown in the lower part of the figure, where the orbital resolved $\varepsilon_2(\omega)$ is depicted for three different levels of Peierls distortion, i.e., PD = 1, PD = 1.1, and PD = 1.2.

Optical properties are not only important for photovoltaics. They are also crucial for PCMs, which can be employed for rewritable optical data storage[12,95] but also photonic switches,[96,97] metasurfaces, and other areas of adaptive optics. The trends in Figures 7, 8, and 10 already show systematic trends for the size of the optical absorption $\varepsilon_2(\omega)$. Increasing ES and ET for metavalent solids decreases the efficiency of photon absorption, accompanied by an increase in the bandgap. The bandgap increase can be realized via increasing charge transfer or via increasing Peierls distortion. The relationship between Peierls distortion and change in optical properties had already been suggested more than 10 years ago by Huang and Robertson.[98] While the amorphous phase is characterized by a pronounced Peierls distortion, the crystalline phase is characterized by a much smaller distortion and hence smaller bandgap as well as stronger optical absorption. This explains the pronounced contrast between the amorphous and crystalline state. While much of this relationship has already been discussed in this paper,[98] the present review discusses this within the systematic framework of quantitative quantum chemistry, which enables detailed predictions for property trends and interesting discontinuous property changes upon crossing the borders between different bonding mechanisms. Before discussing such opportunities, we would like to sketch another recent publication, which provides somewhat surprising insights.

PCMs need to fulfill a plethora of requirements. Besides the pronounced optical or electrical contrast of the amorphous and crystalline state, it is also important to realize rapid transformation processes. Crystallization is usually the time-limiting step. It is thus interesting if clear dependencies of crystallization speed on stoichiometry can be identified. This should help to determine potential speed limits for PCMs,[99–101] relevant to judge the potential for different application scenarios. In the search for systematic property trends, PCMs along the tie-line between GeTe and GeSe, GeTe and SnTe as well as GeTe and Sb_2Te_3 have been studied.[102] Key findings are presented in **Figure 12**, where a pronounced increase of the minimum time to crystallize an amorphous phase is shown upon replacing Te by Se in the GeTe–GeSe tie line. On the contrary, replacing Ge by Sn in the GeTe–SnTe tie line decreases the minimum time to crystallize significantly. Depicted in Figure 12, these trends indicate that the fastest PCMs are located in the lower right corner of the metavalent regime. This finding is not only interesting since it demonstrates the potential of the concept presented here to predict relevant material properties. Figure 12 also offers a scientific surprise. Crystallization entails the processes of the nucleation of crystalline grains in an amorphous matrix and the subsequent growth of these grains. Hence, one would assume that the properties and bonding of the amorphous phase are as relevant as the properties (and bonding) of the crystalline phase. Indeed, modern theories of glasses stress the energy landscape of the glassy state and its relevance for many glass properties including its crystallization kinetics.[103] Interestingly, the coordinates in Figure 12 exclusively describe the bonding of the resulting crystalline phase, while the amorphous phases of chalcogenides discussed here are all covalently bonded and hence reside in the red region of the map. We hence encounter the paradox situation that for the chalcogenides

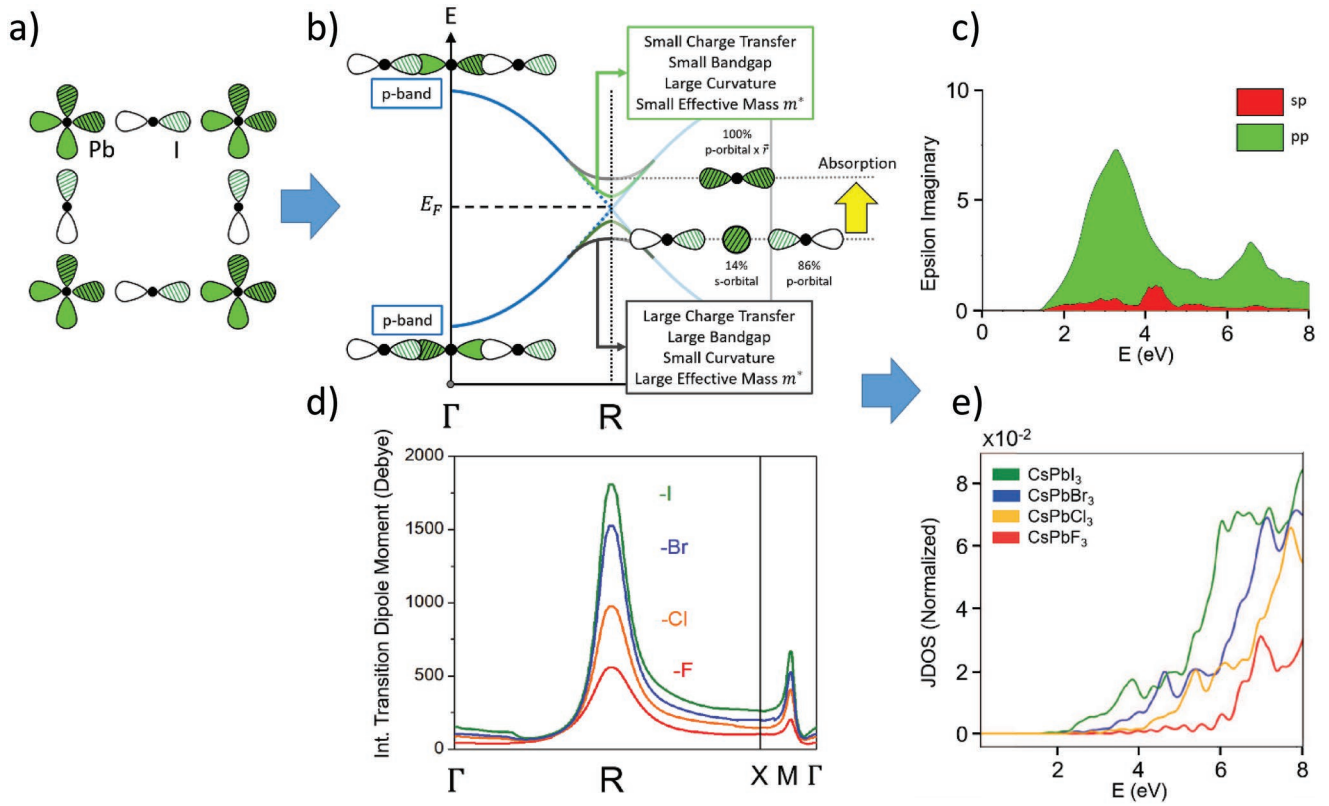

Figure 11. Bond formation and resulting band structure as well as optical properties in $CsPbI_3$. Atomic p orbitals of Pb and I responsible for bond formation are depicted on the left-hand side (1D representation). The atomic arrangement is characterized by small electron transfer and the formation of σ-bonds between adjacent atoms. These σ-bonds are occupied by about half an electron pair (ES ≈ 1), resulting in a metallic band (dashed blue band). However, the electron transfer creates a bandgap at *R* (green/gray band). At Γ, the p–σ states are perfectly bonding (valence band) or antibonding (conduction band), and involve equally the Pb p and I p orbitals (left). At the *R* point, the top of the valence consists of 86% I p and only 14% Pb s (right). The symmetry is such that all interactions are (weakly) bonded. Upon absorption, the transition occurs at the bottom of the conduction band, i.e., 100% Pb p. The parity of this orbital is odd, but the product with the dipolar operator, denoted as $\hat{r}$, makes the state fully symmetric. Therefore, the absorption transition is allowed to this state from both Pb s and I p components of the valence band. The relative contribution of these orbitals to the valence band at the *R*-point, and the larger overlap between neighboring p orbitals is responsible for the much larger p–p absorption. This contribution at the *R*-point shows a clear chemical trend, i.e., it goes down from iodine to bromine, chlorine, and fluorine perovskite. This decrease is attributed to a smaller overlap of the halogen and Pb p states, while the joint density of states has the same form and maxima for all four lead perovskites and is only shifted in energy. Reproduced with permission.[6] Copyright 2021, The Authors, published by Wiley-VCH.

discussed here, the crystallization speed is governed by the final state of the crystallization process and not the initial, a rather surprising finding indeed.

We finally note that the same concepts presented above can also be utilized to tailor thermoelectrics based on chalcogenides as discussed, e.g. in ref. [104]. The examples presented above demonstrate that ES and ET are powerful property predictors. It is tempting to extend this design approach to other properties such as effective masses, the chemical bond polarizabilities, or measures of anharmonicity like the thermal expansion coefficient. Such opportunities will be sketched in Section 7.

6. Why Should Metavalent Bonding be Defined as a Novel Bonding Mechanism?

In the last section, we have focused on the two quantum chemical bonding descriptors (ES and ET) as property predictors. With these two quantities, systematic trends for several band structure related properties in metavalent solids could be explained and predicted. Yet, one can ponder if it is really necessary to introduce metavalent bonding as a novel, fundamental bonding mechanism, instead of defining it, e.g., as a special type of covalent bonding or a mixture of covalent and metallic bonding. Interestingly, Shaik and co-workers have recently suggested different criteria which help to answer the question if and how a new class of bonding should be defined. They have argued that "the prerequisites for legitimately defining a group of bonds as a new class of bonding should be the affirmative answers to the following key questions: 1) Do the bonds belonging to the new class have clearly different features than bonds that belong to formerly defined classes? 2) Is the definition of the new class useful, and does it stimulate chemists to make new predictions?"[105]

Concerning the classification of bonding mechanisms, it is important to clarify which bonding mechanisms are already well-established. Textbooks on bonding in solids usually define the following types of bonding: metallic, ionic, and covalent,

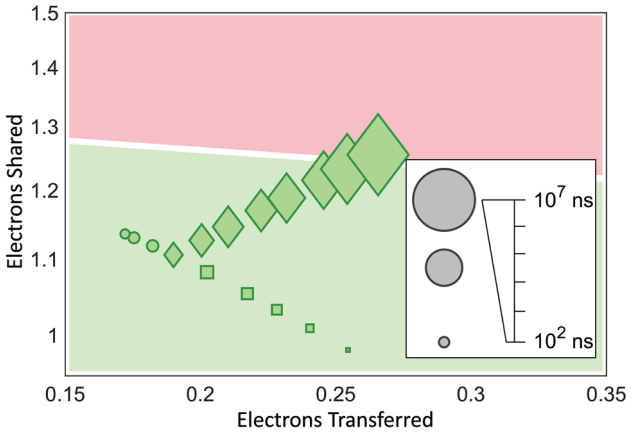

Figure 12. Change of crystallization kinetics with bonding descriptors. Dependence of the minimum crystallization time τ (a) upon two chemical bonding descriptors (ES and ET). A pronounced decrease of the minimum time to crystallize is observed in the metavalent bonding region (green background) between covalent (red) and metallic bonding. Reproduced under the terms of the CC-BY Creative Commons Attribution 4.0 International license (https://creativecommons.org/licenses/by/4.0).[102] Copyright 2021, The Authors, published by Springer Nature.

as well as hydrogen and van der Waals bonding.[78,106] At least the first three types of bonding can be clearly differentiated in terms of their underlying bonding mechanism (see also DAFH orbitals in Figure 4) as well as the resulting material properties. Hydrogen bonding, on the other hand, is often a mélange of other bonding mechanisms. Introducing the term hydrogen bonding is thus possibly more a sign of convenience and of the importance of hydrogen bonding than a chemical necessity. This is quite different for the concept of metavalent bonding discussed here. Metavalent bonding is characterized by material properties which differ significantly from ionic, metallic, and covalent bonding.

Furthermore, unbiased clustering algorithms relate the different property classes obtained to different chemical bonding mechanisms.[80] Besides the clustering by the expectation maximization (EM) algorithm without any human interference, a second approach has been utilized to classify materials for comparison. This method focuses on a somewhat different set of only five material properties (see **Table 6**). These properties have been specifically selected to distinguish different bonding mechanisms based on criteria devised by material scientists.[66] A comparison of the classification employing the two different approaches is illustrated in **Figure 13**. It is striking that there is perfect agreement for the classification by both methods for all materials which employ metallic, covalent, or metavalent bonding mechanisms.

This confirms that metavalent bonding is characterized by a unique portfolio of properties, a prerequisite to introduce a new bonding mechanism according to Shaik and co-workers. However, there is additional evidence that metavalent bonding embodies a bonding mechanism which is distinctively different from metallic, ionic, and covalent bonding. Experiments utilizing laser-assisted field evaporation, as employed in atom probe tomography, reveal that metavalently bonded solids show an unconventional bond rupture. While solids usually only show a low probability of multiple fragments, i.e., a small likelihood of forming more than one single fragment upon bond rupture, metavalently bonded solids are characterized by a much higher probability.[107]All solids which employ metavalent bonding, classified according to the properties listed in Table 6, are characterized by a high probability to form multiple fragments. Hence, the unconventional bond rupture provides further support for a distinct type of bonding in metavalent solids.

Interestingly, the quantum chemical bonding descriptors (ES and ET) also support the view that metavalent bonding is different from covalent, metallic, and ionic bonding. This has been shown in Figure 3, where these two quantum chemical bonding descriptors have been employed to separate metallic, ionic, and covalent bonding. In this map, metavalent solids are characterized by a unique range of ES and ET values. The electron transfer is small or moderate and adjacent atoms share close to one electron, i.e., half an electron pair (2c–1e bonding). This unconventional bonding scheme is also visible in Figure 4, where the corresponding DAFH orbitals are depicted. They differ significantly from metallic, covalent, and ionic DAFH orbitals. Hence, it seems fair to say that the prerequisite defined by Shaik and co-workers to classify metavalent bonding as a new bonding mechanism is fully met.

Possibly the more interesting question raised is whether the new bonding class is useful and stimulates chemists and other scientists to make new predictions? Indeed, the notion that metavalent bonding is a distinct bonding mechanism, immediately raises a number of interesting questions and provides interesting hypotheses.

If metavalent bonding is a distinct bonding mechanism, which differs from ionic, metallic, and covalent bonding then there ought to be borders between metavalent bonding and its neighbors in the map of Figure 3. With distinct properties characteristic for different bonding mechanisms, one may wonder which property changes will provide evidence for a change of bonding? This question has been answered already

Table 6. Different types of chemical bonds and their characteristic properties. No set of properties (of any bond type) is a linear combination of the other bond types. This provides strong evidence that these four bond types are indeed unique and not a combination or mixture of the other bonds. Adapted from ref. [80].

	Ionic (e.g., NaCl)	Covalent (e.g., Si, GaAs)	Metavalent (e.g., GeTe)	Metallic (e.g., Cu, NiAl)
Electronic conductivity σ	Very low (< 10^{-8} S cm^{-1})	Low-moderate (10^{-8} to 10^{2} S cm^{-1})	Moderate (10^{1}–10^{4} S cm^{-1})	High (>10^{5} S cm^{-1})
Number of nearest neighbors	4 (ZnS), 6 (NaCl), 8 (CsCl)	8-N rule typically satisfied	8-N rule not satisfied	8 (bcc), 12 (hcp/fcc)
Optical dielectric constant ε_∞	Low (≈2–3)	Moderate (≈5–15)	High (>15)	–
Born effective charges Z*	Low (1–2)	Moderate (2–3)	High (4–6)	Vanishes (0)
Grüneisen parameter g γ_{TO}	Moderate (2–3)	Low (0–2)	High (>3)	Low (0–2)

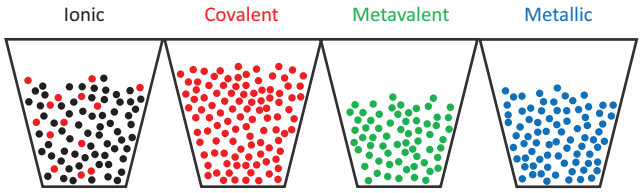

Figure 13. Overview of the clustering results for four clusters. Each bucket represents a cluster found by the EM algorithm, while the colors indicate the bonding type of the corresponding compound by the criteria of Table 6. Black: ionic, red: covalent, green: metavalent, blue: metallic. Adapted under the terms of the CC-BY Creative Commons Attribution 4.0 International license (https://creativecommons.org/licenses/by/4.0).[80] Copyright 2022, The Authors, published by American Association for the Advancement of Science.

for the transition between metavalent and covalent bonding. Guarneri and co-workers have explored this border by studying pseudo-binary alloys of GeTe–GeSe, Sb_2Te_3–Sb_2Se_3, and Bi_2Se_3–Sb_2Se_3.[108] For all three systems studied, a sudden change in several properties, including the optical absorption $\varepsilon_2(\omega)$, the optical dielectric constant ε_∞, the Born effective charge Z^*, and the electrical conductivity σ, as well as the bond breaking behavior is evidenced for a critical Se or Sb concentration, respectively. Data for the pseudo-binary line of GeTe–GeSe are shown in **Figure 14**, which displays data for the optical dielectric constant ε_∞. While amorphous compounds show a continuous change of the optical dielectric constant ε_∞, for the crystalline compounds a sudden jump is observed, even for the same stoichiometry, e.g., for compounds close to $GeSe_{.5}Te_{.5}$. Upon the transition from the hexagonal to the rhombohedral phase of this alloy, a significant increase of ε_∞ is observed, which cannot be explained simply by a change in atomic density, as described by the Clausius–Mosotti equation (dashed line in Figure 14b). Discontinuous changes have also been observed for the room temperature conductivity σ and the Born effective charge Z^*. The sudden change in material properties is also mirrored in sudden changes of bond rupture. The crystalline compounds with orthorhombic and hexagonal structure in Figure 14 are characterized by a much lower probability of multiple events, as observed for ordinary covalent compounds. All solids, however, which show the characteristic material properties of metavalent compounds also reveal the characteristic bond rupture in laser-assisted field emission, i.e., a high probability of multiple events. Hence, the transition between metavalent bonding and covalent bonding is evidenced by a number of clear property changes, as expected for a significant bonding change.

The transition between metavalent and ionic bonding has also been studied recently. Maier et al. have explored systematic property changes in lead monochalcogenides.[81] This study has shown that PbTe, PbSe, and PbS are metavalently bonded, while PbO is iono-covalently bonded, i.e., governed by rather polar covalent bonds. Again, systematic property changes have been found. Nevertheless, it is very difficult for this material system to study a dense stoichiometry grid along the transition between metavalent and ionic bonding. Such a transition would hypothetically occur for alloys of PbS and PbO. Yet trying to produce such compounds is not possible due to decomposition and generation of toxic SO_x. Hence, the observed property changes again are indicative for distinct bonding changes, but so far it has not been possible to investigate compounds in close vicinity of the border, as explored for the metavalent–covalent border.

We are not aware of a systematic study of the transition between metavalent and metallic bonding, but can already suggest which physical properties should be fascinating to explore. Two characteristics seem particularly interesting, the Born effective charge and the tendency toward local atomic distortions. While metavalent solids are characterized by high values

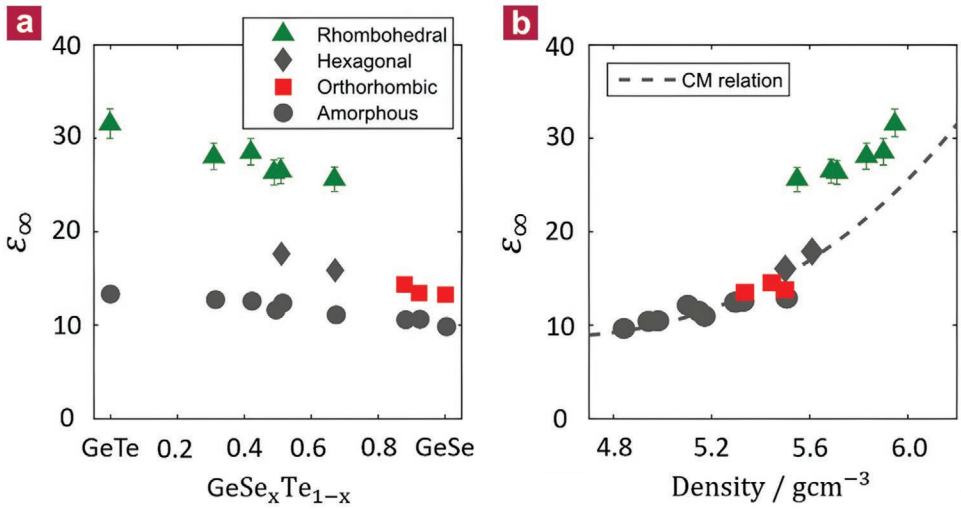

Figure 14. Optical dielectric constant ε_∞ along the pseudo-binary line between GeTe and GeSe. a) ε_∞ as a function of stoichiometry. The rhombohedral phase, found up to 70% Se, is characterized by large values of ε_∞, which exceed the value of the corresponding amorphous phases by more than 100%. Between 50% and 70% Se content, the rhombohedral phase is metastable and transforms into a hexagonal phase upon further heating. This transition is accompanied by a pronounced drop in ε_∞. b) ε_∞ plotted as a function of density. The data for the amorphous, orthorhombic, and hexagonal phases follow the Clausius–Mossotti (CM) relation (dashed line), which relates ε_∞ and the mass density of the material. Only the rhombohedral phase shows an excess of the electronic polarizability and hence ε_∞, characteristic for metavalent bonding. Reproduced with permission.[108] Copyright 2021, The Authors, published by Wiley-VCH.

of the Born effective charge Z^*, which provides a measure of the chemical bond polarizability, good metals have sufficiently mobile charge carriers to screen any dynamic dipole moment. This implies that there must be a transition between high values of Z^* at the moderate room temperature values of the electrical conductivity and vanishing values of Z^* at even higher conductivity values found for good metals. The precise nature of this expected transition, however, has not yet been studied.

Many metavalent solids furthermore possess Peierls-like atomic distortions. These distortions reduce the DoS in the vicinity of the Fermi level. Will a similar reduction in the DoS exist for metals close to the border between metallic and metavalent bonding? This would be exciting, since it would indicate that the proximity of the border would already cause emergent phenomena which signal the proximity of this border.

In the preceding discussion, various examples were discussed showing how the concept of metavalent bonding provides ideas for further studies and the search for systematic property trends, meeting the expectation of Shaik et al. that a new class of bonds should inspire new predictions. Hence, it seems justified to use a bonding classification for the chalcogenides discussed here, which stresses the dissimilarities from metallic, ionic and covalent bonding. Indeed, in the last 50 years, a number of different bonding mechanisms have been discussed to explain different aspects of these solids. We will briefly introduce these terms and their definition and will address whether they seem appropriate to explain and predict relevant properties and phenomena.

The unconventional properties of chalcogenides like GeTe, Bi_2Se_3, PbTe, PbSe, and related compounds have already intrigued chemists and physicists for several decades. Hence, it is not surprising that concepts of chemical bonding have been utilized to explain these properties. Krebs already pointed out that the atomic arrangement in solids like Sb or GeTe was incompatible with ordinary (2c–2e) covalent bonding.[47] He suggested to call the underlying electronic configuration "resonant bonding," since the atomic arrangement of these solids can be described as a superposition of two (or more) different limiting cases. The term "resonant bonding" was later also employed by Lucovsky and White and one of the authors of the present manuscript to explain the unusual properties of crystalline GeTe and other PCMs.[48,49] While it seems obvious to invoke a special bonding mechanism to explain the unconventional properties of crystalline PCMs, the choice of wording "resonant bonding" seems unfortunate. The term "resonant bonding" immediately reminds many scientists of the bonding scenario in aromatic compounds such as benzene and possibly even solids like graphite and graphene. This association dates back to Linus Pauling's famous explanation of the atomic arrangement and physical properties of benzene.[17] Yet, the properties of the chalcogenides mentioned above have little, if anything in common with the properties of benzene or graphite. This can be seen, e.g., for the anharmonicity of the bonds, as characterized by the Grüneisen parameter, the volume dependence of the phonon frequencies. This quantity is very high for chalcogenides like PbTe and GeTe, indicative of the close proximity of an instability, while a much smaller and rather normal Grüneisen parameter characterizes graphite.[66] Obviously, the chemical bonding in graphite and benzene is rather harmonic, but quite soft and anharmonic in metavalent solids. This anharmonicity is closely related to the bond order of about 0.5, significantly smaller than the value of 1 for a normal covalent bond (2c–2e). Considerable differences are also observed upon bond rupture in laser-assisted field evaporation.[109] While the metavalent chalcogenides are characterized by a large number of multiple events, the probability of such events is rather low for carbon nanotubes, i.e., rolled up sheets of graphene. This is further evidence of pronounced difference in bonding. Finally, in the map depicted in Figure 3 also clear differences between bonding in graphite and GeTe are obvious. Graphite is characterized by 2c–3e bonding, i.e., both a σ-bond filled with one electron each from the two sp^2 hybrids of adjacent atoms and half an electron each from two p_z orbitals of these atoms, forming a half-filled π-bond. Hence, the term "resonant bonding" to explain the unconventional properties of the chalcogenides discussed here should indeed be abandoned.

Frequently also lone pairs have been invoked to explain properties of monochalcogenides such as PbTe, PbSe. and others. The key idea behind this notion is the expected significance of the Pb $6s^2$ orbital for these chalcogenides. Indeed, lone pairs contribute to the atomic interaction and arrangement in molecules like NH_3 and H_2O, where they influence, e.g., the H—O—H bond angle and help to explain the bond angle of 109°, which differs significantly from the bond angle of 180° expected for a linear molecule without lone pairs. For the massicot structure of PbO, where four oxygen ions are located in one half-space of the lead cation, i.e., an arrangement which is not favored to maximize the electrostatic energy, a Pb s^2 lone pair state has been suggested as an explanation.

Such a lone pair should play a prominent role if the Pb $6s^2$ state is located close to, but below the Fermi energy E_F. In this case, lead has the oxidation state Pb^{2+}, i.e., the p orbital of Pb is depopulated. **Figure 15** shows the DoS for the formal valence electrons of Pb and Te for rock-salt-structured PbTe with three rather different lattice constants. In the first version (lattice expansion of 50%, i.e., a factor of 1.5), orbital overlap is minimized and the energy levels of the different atoms have been obtained from a solid with an artificially large interatomic spacing, i.e., a lattice constant of 9.85 Å instead of 6.57 Å. In this case, the s electrons of Pb and Te are completely filled far below E_F, while there is apparently already some Te p Ge p orbital overlap. In Figure 15b, the DoS is depicted for a more realistic scenario, which includes a larger orbital overlap due to the smaller distance of adjacent Pb and Te atoms (lattice expansion of 25%, i.e., a factor of 1.25). This already shows that the overlap between Pb p and Te p orbitals ensures that there is a finite population of Pb p states populated below E_F. Finally, Figure 15c shows the DoS as obtained by DFT calculations. This figure shows that there is significant overlap between the p states of Te and Pb. The p states of Pb are occupied with 1.87 electrons (as obtained by the orbital-resolved IDOS), in contrast to the lone pair model, which assumes a vanishing occupation of this state.

The partial occupation of the Pb p state is also compatible with the moderate electron transfer between Pb and Te, which is determined to 0.694. This leads to a renormalized electron transfer of 0.347 (after division by the formal oxidation state of 2), as is seen in the map depicted in **Figure 16**a. The analysis

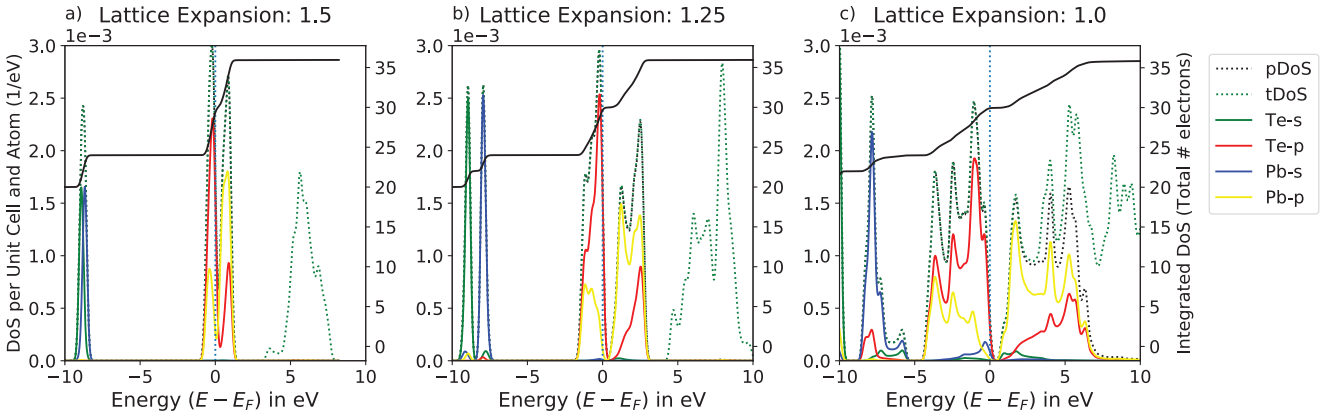

Figure 15. Orbital-resolved DoS per unit cell and atom of PbTe with a lattice expansion factor of 1.5, 1.25, and 1.0 in (a)–(c), respectively. This lattice expansion is explored to investigate the impact of reduced orbital overlap (upon lattice expansion). pDoS describes the sum of all projected DoS values, whereas tDoS is the total DoS. They are shown with black and green dashed lines, respectively. The right *y*-axis (black) shows the integrated DoS.

of the corresponding DAFH orbitals further corroborates this view. As shown in Table S1 of the Supporting Information, the dominant contribution to bond formation is the Pb p Te p orbital overlap which contributes 0.25 electron pairs out of 0.40 electron pairs, while the Pb s Te p orbital overlap only contributes 0.05 electron pairs. This confirms that the bonding is dominated by p–p orbital overlap, while the contribution of Pb s^2 state is quite small.

One can now relate bonding to properties to clarify, which properties are governed by which orbital contribution. This can be done in a straightforward manner for the dielectric function $\varepsilon_2(\omega)$, as shown in Figure 8c. Decomposing $\varepsilon_2(\omega)$ into different orbital contributions reveals that the dielectric function is governed by p–p transitions, while s–p transitions only play a minor role. The larger the p–p orbital overlap, the stronger the maximum of the optical absorption, i.e., maximum of $\varepsilon_2(\omega)$. This p–p orbital overlap also leads to small effective masses of valence band maxima and conduction band minima (see Figure 8b). Again, this finding is not compatible with the prominent role of the Pb s state, predicted in the lone pair model.

Finally, one can analyze how the Pb s and p states contribute to different lead chalcogenides. This is depicted in Figure 16a. The figure shows the connecting line between Sb and PbS in the ES-ET-map and the connecting lines of their s and p orbital contributions. The slopes of the connecting line of the whole bond and the p orbital contribution are both at around –0.5. The slope of the connecting line of the s orbital contribution instead is at 0.05 only. The points for PbTe and PbSe and their orbital contributions lie almost exactly on those lines.

Therefore, the Pb s state slowly increases in significance with increasing electron transfer ET, as expected. Yet, the more pronounced change is the strong reduction in the p–p orbital overlap. It is this reduction, which governs the decrease of the optical absorption or the increase of the effective mass m^* with increasing electron transfer. A similar conclusion can be drawn from a quantum-chemical analysis of bonding for the α-, β-, and γ-phase of GeTe, which differs in their amount of distortion away from a perfect octahedral arrangement. Their map positions of the whole bond and orbital contributions are shown in Figure 16b. Whereas the absolute contributions of p-orbitals changes drastically from the β- to the γ-phase, the s orbital contribution stays the same for all three phases and is much smaller. Therefore, the s orbital plays a minor role in the changes of properties.

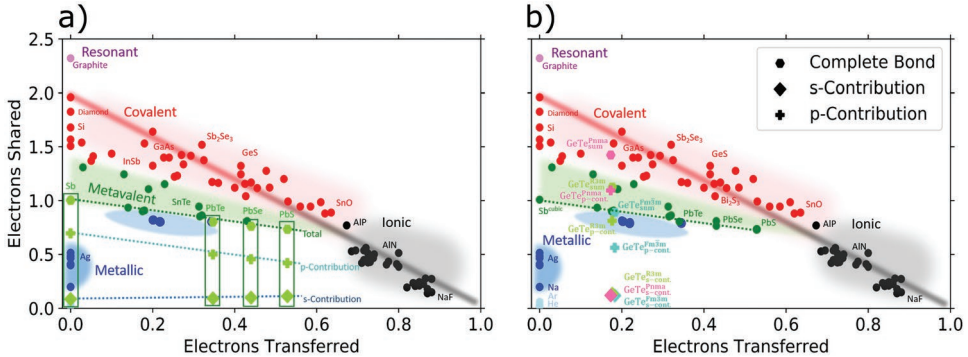

Figure 16. a) The map positions for Sb in its cubic phase, PbTe, PbSe, and PbS (denoted by the hexagon symbol) among other materials (denoted by dots) for comparison. In (a) and (b), the ES values are split into their p and s orbital contributions, respectively (denoted by diamonds and crosses). The green, light blue, and dark blue line in (a) connect the compounds Sb and PbS and their p and s orbital contributions, respectively. In (b), the map positions for the α- ($R3m$), β- ($Fm3m$) and γ- ($Pnma$) phase are shown (denoted by the hexagon symbol).

In summary, the special bonding configuration, i.e., half-filled σ-bond of p orbitals can explain the electronic band structure and resulting material properties such as the optical absorption and anharmonicity of the lattice, without postulating a special role of Pb s^2 states. This is supported by quantum chemical calculations, which find no evidence for a prominent role of the Pb s^2 states in these monochalcogenides.

It seems even more misleading to characterize the bonding of GeTe and other crystalline chalcogenides and PCMs as hypervalent bonding in nature and, namely, in this case, as 3c–4e bonding. Indeed, there are a number of molecules, where electron-rich 3c–4e electron bonding has been postulated and confirmed. Well-known examples include XeF_2 and SF_4. These molecules can be analyzed by the same quantum-chemical bonding analysis that we have employed for GeTe. In the map of Figure 3, we now also depict these 3c–4e bonded molecules. These molecules are located in a very distinct region of the map, remote from other regions, and in particular far away from metavalently bonded chalcogenides. This figure depicts unequivocally that the bonding in electron-rich (3c–4e) molecules has nothing in coming with the bonding mechanism in the chalcogenides discussed here. Hence, as argued already in considerable detail in Section 2, there is no evidence of the participation of four electrons between three centers. Instead, the quantum-chemical bonding analysis based on DAFH orbitals, the bond order analysis as well as the delocalization indices confirms a 2c–1e bonding between Ge and Te, so involving half of an electron pair, governed by p–p orbital overlap. Interestingly, the understanding that cubic monochalcogenides such as GeTe form an octahedral arrangement with bond order ½ was already known in the early 80s of the last century, as referenced in the Landolt Börnstein database,[110] but not discussed as an unconventional bonding mechanism, in contrast to the view offered here. Finally, whether two aligned Ge–Te 2c–1e bonds may be rather envisaged as a case of 3c–2e bonding, can be only rigorously excluded (or confirmed) by employing the three-center formulation of the delocalization indices.[111] This should be an interesting object of investigation in forthcoming studies.

The concept of 3c–2e bonding is usually discussed as a special form of covalent bonding.[112] Yet, the notion of covalent bonding for the metavalent solids discussed here seems inadequate, since it ignores the unique property portfolio of this material class and its distinct border with ordinary covalent compounds, supported by rigorous classification algorithms. Hence, it seems crucial to use a terminology which adequately reflects the unique material properties, the special position in the bonding map, and the unusual bond rupture. This is our reasons to use a distinctly different name, i.e., metavalent bonding.

There is one more recent concept which explains unconventional aspects of bonding, which has been developed by Shaik and co-workers.[113] This concept has been established to explain the atomic arrangement and energetics of molecules in which it is the covalent–ionic valence bond resonance that stabilizes the molecule. The concept is based on a quantum-chemical characterization and has been related to experimental manifestations such as activation energies for atomic exchanges. The criteria used in ref. [105] have helped to shape our arguments, why metavalent bonding is a novel and unique bonding mechanism.

It is tempting to argue that metavalent bonding is just another name for charge shift bonding. To confirm or refute this hypothesis, it would be ideal to have a large set of solids, which have been characterized as either metavalent or charge-shift bonding. Unfortunately, the corresponding cut set is rather small. This is due to the fact that charge shift bonding has been mainly explored for molecules, while metavalent bonding has been developed to explain systematic trends for solids. Furthermore, the concept of charge shift bonding relies on quantum-chemical arguments based on the size of the resonance energy upon charge shifting. Metavalent bonding instead started as an attempt to classify relevant material properties and built a bridge between bonding schemes and the resulting (measureable) material properties. Hence, the algorithm to classify a molecule or solid as employing metavalent or charge-shift bonding clearly differs. Yet, these differences do not suffice to conclude that the resulting material classes must differ. A comparison of the list of materials which utilize charge shift and metavalent bonding shows that there is a much broader range of materials, which have been characterized as members of the group of charge-shift bonded molecules. Molecules with 3c–4e bonding such as XeF_2 or even with 2c–2e bonding like F_2 are listed in this category. However, their bond order is much larger than ½ and hence they do not fall in the class of metavalent systems since they would not be located in the green region of Figure 3.[114] A definitive answer on the similar or quite distinct nature of charge shift and of metavalent bonding could be obtained by exploiting the recent extension of the electron distribution functions (EDFs) to the (periodic) solid state.[115] EDFs can be envisaged as real space analogs of Pauling resonance structures. In agreement with what is known in finite systems, ionic compounds display narrow EDFs that get wider as covalence sets in. Relative to standard covalent bonds, charge-shift bonds should be characterized by large and enhanced weights of the ionic structures, while metavalent bonds might be predicted to have (much) wider EDF distributions than covalent bonds, but similarly centered around the (more) shared structures. Clearly, this kind of investigation goes beyond the scope of the present review, but it looks like a very interesting subject of study for forthcoming investigations. Regardless of the possible, yet unlikely, similarity with charge shift bonds, it is highly desirable to expand the class of metavalent solids to gain a better understanding of the breadth of this class of materials.

In recent years, a number of studies have attributed striking observations to metavalent bonding. In the following, we provide a short and possibly incomplete summary. The concept of metavalent bonding has been used to explain exceptionally low lattice thermal conductivity in the 2D $Bi_2Si_2Te_6$ semiconductor,[116] p-type polycrystalline rhombohedral $(GeSe)_{0.9}(AgBiTe_2)_{0.1}$,[117] as well as TAGS-x thermoelectric materials[118] and several chalcopyrites,[119,120] which facilitates attractive thermoelectric performances. In particular, favorable properties of chalcogenides such as PbTe and other octahedral-like chalcogenides have been attributed to the band structure, which is due to the half-filled σ-bond formed upon overlap of adjacent p orbitals characteristic for metavalent bonding.[84,85] This has also been concluded by a recent paper which has experimentally demon-

strated that metavalently bonded GeSe leads to favorable thermoelectric properties.[117] Tolborg and Iversen even went one step further and related trends for chemical bonding in half-Heusler semiconductors to trends in relevant material properties including the thermoelectric power factor and the Fermi surface complexity factor.[121] In addition to that, several phenomena have been attributed to metavalent bonding, such as the formation of dynamic dipoles in PbTe due to the softening of the TO branch,[122,123] the absence of translational shear fault defects in some layered chalcogenides,[124] and the switching mechanism in amorphous ovonic threshold switching materials under an electric field.[125] So-called photoenhanced metavalent bonding has been observed in pump-probe experiments by Yang et al.[126] Under high pressures, metavalent bonding emerges in several compounds. For example, in orpiment, where it is accompanied by the softening of several vibrational modes and the decrease of the phonon bandgap,[127] in p-type layered SnSe[128] and in the compressed rhombohedral phase of $SnSb_2Te_4$.[129] Furthermore, metavalent bonding has been employed to explain the broadening of Raman lines with increasing temperature in GeTe[130] and in amorphous Sb_2Se_3, where the emergence of a superconducting phase has been attributed to it. The role of metavalent bonding in high pressure dynamical studies is reviewed in ref. [131] using theoretical and experimental data.

Besides, the metavalently bonded materials already mentioned, As_2Te_3 has been also been proposed to employ this unconventional bonding mechanism.[132] Interestingly, metavalent bonded solids are also particularly prone to disorder and anharmonic effects. This is presumably closely related to the weak bonds which characterize these materials. As a consequence, it is rather easy in many of these compounds to create defects such as vacancies.[133] These vacancies have been shown to have a strong impact on transport properties, such as the electrical and thermal conductivity.[134–136] Disordered vacancies can even lead to disorder-induced localization and exotic transport phenomena.[137,138] A recent study has addressed the question in which compounds such localized states can be expected at the Fermi energy.[139]

While ES and ET are the bonding descriptors which first made the distinction between metavalent and other types of bonding visible, they are not the only quantities that can uniquely define this new bonding type. Other approaches have been developed using Hirshfeld surface analysis[140] or the chemical pressure formalism.[141] The authors of ref. [140] conclude that the Hirshfeld surface analysis provides quantum level descriptors that can be used for rapid screening of crystallographic data to identify potentially new "metavalent" solids with novel and emergent properties.

7. Outlook

As already mentioned in closing the last section, it would be highly desirable to identify further metavalent solids. At present, metavalent bonding has been confirmed for crystalline solids like GeTe, SnTe, PbTe, PbSe, PbS and their alloys, Sb_2Te_3, Bi_2Te_3, and Bi_2Se_3, as well as $AgSbTe_2$.[142] All of these materials possess an unconventional property portfolio including high values of the chemical bond polarizability (Born effective charge Z^*), large values of the Grüneisen parameter for optical phonons, indicative for rather anharmonic bonds, high values of the optical dielectric constant ε_∞, a measure of pronounced electronic polarizability, and a number of nearest neighbors incompatible with ordinary covalent bonding (8-N rule) as well as an unusual bond rupture upon laser-assisted field evaporation. These compounds are characterized by the overlap of half-filled p orbitals leading to an electronic configuration, where adjacent atoms form half an electron pair, i.e., share one electron in total. This configuration extends for each atom involved in three almost orthogonal directions, leading to a 3D network of metavalent bonds. Yet, to realize a metavalent bond in the green region of the map of Figure 3, it is sufficient to form half an electron pair, i.e., share one electron in just one direction. This configuration is encountered for halide perovskites like $CsPbI_3$, where the iodine atom forms metavalent bonds and shares an electron each with both Pb neighbors.[6] This electronic configuration explains the favorably strong optical absorption and small effective masses as discussed in Section 5. While iodine atoms only form one metavalent bond in a single direction, cubic GeTe and cubic Sb form a 3D network of metavalent bonds. It is interesting to search for property differences between networks of metavalent bonds of different dimensionality. In this context, one can ponder if there are also similar networks in 2D. Solids like $EuTe_3$ and related tellurides, or the orthorhombic *Cmcm* phase of SnSe might be candidates for such a bonding scenario.

The halide perovskites are also interesting for a second reason. In halide perovskites with stoichiometry ABX_3, two different bonding mechanisms prevail. The A—X bond is clearly ionic, while the B—X bond fulfills the property criteria of metavalent solids listed above (large value of Z^* for B—X bond, coordination number of 2 for the halogen atom, strong optical absorption due to pronounced p orbital overlap of B- and X-atom). This indicates that a metavalent-like bonding situation can also be encountered in a ternary compound. Regarding the goal of designing materials, this conclusion raises interesting questions and research opportunities. Can we relate certain material properties of a solid to specific bonding configurations, in the spirit of the 3d map shown in Figure 6? A clear answer to this question is important in order to adequately assess the design concept presented here in terms of its applicability to larger material classes, in particular those solids which contain more than just one or two different elements.

A second exciting opportunity is the exploration of the border between metavalent bonding and its neighbors, i.e., covalent, ionic, and metallic bonding. We have already discussed the pronounced property changes at the border between metavalent and covalent bonding. It is most likely no surprise that an unconventional solid like hexagonal Ge_4Se_3Te is found in close proximity of this border.[143] So far, few systematic studies of the border between metavalent and ionic border have been reported. For the border between metavalent and metallic bonding, first reports and predictions are just emerging. This border looks particularly interesting, since it provides a rarely studied perspective on the nature of metal–insulator transitions. Metal–insulator transitions have fascinated physicists for decades and continue to cause their

attention. Upon gradually alloying metavalent compounds like $AgSbTe_2$ and metallic alloys like In_3SbTe_2 or $AgSnTe_2$, an MIT transition can be realized. We expect interesting data for the temperature dependence of the electrical conductance upon changing stoichiometry. The Born effective charge Z^*, which is rather pronounced for metavalent solids, but vanishes for good metals, should also show an interesting dependence upon stoichiometry.[80]

As mentioned in Section 1, the nature of the chemical bond became a hot topic in chemistry, when quantum mechanics became available. In the last decades, the tools have finally become available for a precise, quantitative description of solids based on quantum-chemical calculations. Figure 4 provides a visual presentation of the differences between covalent, metallic, and metavalent bonding in terms of the spatial distribution of the DAFH. Yet, one can ponder if a more intuitive explanation of the nature of metavalence is possible. Covalence is characterized by electron localization via electron pair formation, while metallic bonding is enabled by electron delocalization and the concomitant reduction in kinetic energy. Metavalent bonding is apparently the competition zone of electron localization and electron delocalization. As a consequence, subtle changes in atomic arrangement such as changes in the size of the Peierls distortion have an impact on the degree of electron localization and accompanying changes in electrical conductivity, as well as other physical properties discussed in Section 5. Yet, these property changes can be realized upon a modest change of energy (see Figure 6). Metavalently bonded materials are hence easy to tailor in their properties upon external parameters such as disorder, pressure, and temperature. This dependence is exploited in PCMs through pronounced property changes upon crystallization, but can also be used to tailor thermoelectrics, for example.

The competition between electron localization and delocalization can also help to understand the pronounced dependence of properties of metavalent solids upon reduced dimensions. This is shown in **Figure 17** for thin films of GeTe grown by molecular beam epitaxy (MBE). Upon decreasing film thickness, the Raman frequencies of the optical phonons of the crystalline samples increase, a rather unusual thickness dependence. The amorphous films on the contrary show no similar thickness dependence. The dependence of the vibrational modes with film thickness is accompanied by significant changes of atomic arrangement, which are indicative for an increasing Peierls distortion with decreasing film thickness. The increasing Peierls distortion leads to a reduction of the orbital overlap as shown in Figure 10, leading to a reduction of the maximum of $\varepsilon_2(\omega)$ as shown in Figure 17c. No similar thickness dependence is observed for the amorphous films, which behave like ordinary covalent solids. The thickness dependence of the crystalline sample can be attributed to changes in the competition between electron delocalization and electron localization upon reducing film thickness. With decreasing film thickness, there is increasing electron localization, as evidenced also by increasing values of ES, which explains the concomitant changes in phonon frequency and Peierls distortion. For ordinary covalent bonding, where covalent bonding prevails no similarly pronounced film thickness is expected and found.

All of the solids discussed in the preceding paragraph are governed by σ-bonds with half-filled p orbitals. However, a competition between electron localization and electron delocalization should also be feasible with solids where d electrons prevail in bonding or form σ-bonds of p–d orbitals. This happens in transition metals nitrides and oxides. Interestingly, all transition metal nitrides above SnN, i.e., from TiN to ZnN possess a metallic rock salt structure, which often is the ground state structure for these compounds.[13] Transition metal oxides on the contrary show frequently an insulating ground state.[13] There is thus a striking difference of electron localization comparing the nitrides and oxides of transition metals. It is tempting to relate this to systematic changes of bonding and search for metavalence beyond p-bonded solids.

So far, this outlook has focused on aspects related to metavalent bonding in chalcogenides and related compounds. Yet, there is another perspective one can adopt. The map in Figure 3 is not only offering an interesting perspective in providing a quantitative description of bonds in solids. It also enables predictions of material properties and interesting property trends. One can hence employ this map to search for thermoelectrics, topological insulators, photonic switches, and PCMs. So far, we have reviewed trends for the bandgap E_g and other optical properties like $\varepsilon_2(\omega)$ and ε_∞, but also vibrational properties like the Grüneisen parameter and the chemical bond polarizability (Z^*). Yet, there should be significantly more relevant material properties which should show a clear functional dependence upon the axes which span Figure 3. At the same time, we expect some material properties to be rather independent of the underlying bonding mechanism. High melting temperatures of above 3000 K, e.g., can be realized in covalent (C (diamond) 3900–4300 K),[145] ionic (MgO 3125 K),[146] and metallic solids (W 3687 K)[147]). Hence, studying which relevant material properties are closely related to the quantum-chemical bonding descriptors investigated in this review and which ones are not, hence also offers a much deeper understanding of the origin of important material properties, i.e., if they are closely interwoven with a certain bonding mechanism or not.

The success of the two quantum chemical bonding descriptors ES and ET as property predictors leads to another exciting question. Why are ES and ET such excellent property predictors? Apparently, ES and ET are natural variables for chemical bonds and material properties. The relevance of ET is not so surprising. Previous generations of maps have already utilized the electronegativity difference as a measure of the degree of charge transfer. Comparing maps based on the electronegativity difference (ΔEN) with those based on ET, it seems as if ET is clearly better suited to separate materials with different bonding mechanism. This is presumably due to that fact that ET is a much better measure of charge transfer between adjacent atoms than ΔEN. The success of ES is more telling. ES is closely related to electron–electron interactions including exchange and correlation. The success of ES in describing chemical bonds and material properties indicates that ES is a natural variable for chemical bonding and many properties of functional materials. It seems worthwhile to better understand why these two quantities are so predictive and descriptive.

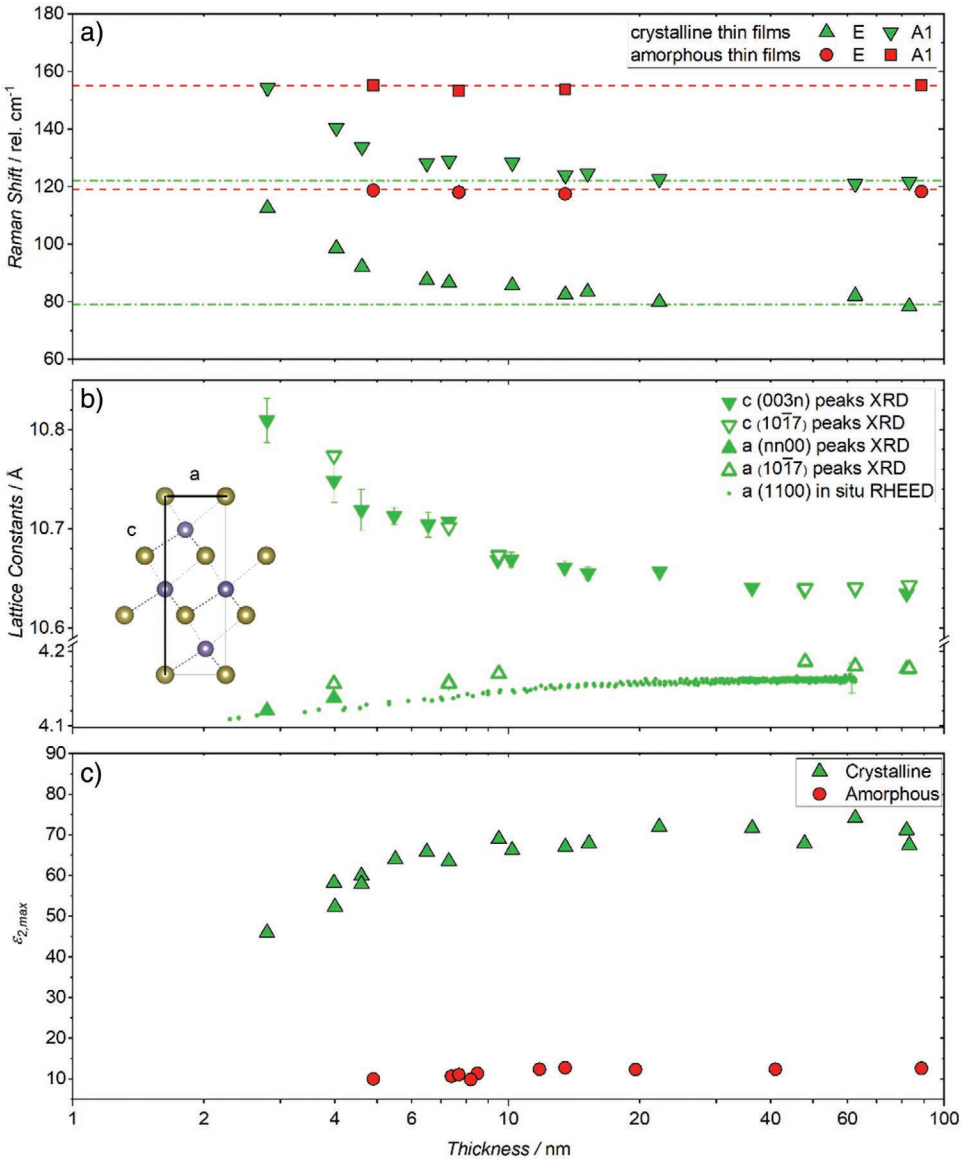

Figure 17. a) Thickness-dependent frequencies of the GeTe Raman modes in the amorphous (red symbols) and crystalline (green symbols) phase. While the frequencies of the amorphous samples are independent of the thickness, the modes are strengthened for ultrathin crystalline GeTe films. B) a in-plane and c out-of-plane lattice constants obtained as a function of film thickness. Closed triangles are calculated from peaks with either $h,k,l = 0$ and open triangles from the reciprocal space maps of the (1017) peaks. Closed points depict the lattice parameter obtained from the reflection high-energy electron diffraction measurement during growth of the 62.5 nm sample. All methods agree that the unit cell is distorted toward higher c and lower a for ultrathin films. Inset drawn with VESTA.[144] c) Maximum value of $\varepsilon_2(\omega)$ as a function of thickness for the amorphous (red) and crystalline (green) samples shows the increased thickness dependence for the crystalline samples.

8. Summary

Many material scientists strive to design advanced functional materials with targeted functionalities. In this review, we have summarized recent attempts to employ quantum chemical bonding descriptors to guide the search for superior materials in chalcogenides and beyond. To this end, DI, ES, and ET as well as DAFH have been introduced. In conjunction with the determination of the bond order as well as the orbital resolved band structure and DoS, these quantities provide a powerful toolbox to quantitatively describe chemical bonding in solids. Hence, ES and ET are precise quantum-chemical bonding descriptors. More importantly, they are also powerful property predictors. They can be utilized to predict property trends for many properties which are band structure related. Hence, they represent the natural variables to translate between the language of chemical bonding and the band structure world of physics.

Interestingly, this search for property trends and their explanation through quantum chemical bonding descriptors also finds evidence for a fundamental bonding mechanism besides ionic, metallic, and covalent bonding, which has been called

"metavalent" bonding. It is characterized by an unconventional property portfolio and a bonding situation where about one electron (half an electron pair) holds together two adjacent atoms. Hence, metavalent solids occupy a special region in a map spanned by ES and ET. This bonding mechanism is also accompanied by an unconventional bond rupture in atom probe experiments. Interestingly, discontinuous property changes are observed at the border between metavalent and covalent bonding and presumably also at the border between metavalent and metallic bonding.

We hope that this review stimulates further studies of systematic property trends in functional materials. While the present study has focused on chalcogenides and p-bonded systems, similar trends and opportunities are expected for other material classes. We are thus optimistic that the interplay of quantum chemistry, material science, and solid state physics can advance our understanding and optimization of advanced functional materials that can help ensure a more sustainable future for mankind.

Supporting Information

Supporting Information is available from the Wiley Online Library or from the author.

Acknowledgements

Funding through the ERS of RWTH Aachen within project neuroIC005 (From Data to Treasure Maps in Materials Science: A Case Study for Data Driven Hypothesis Generation and Evaluation) is gratefully acknowledged. C.F.S. and M.W. acknowledge funding in part from the Deutsche Forschungsgemeinschaft (DFG) via the collaborative research center Nanoswitches (SFB 917) and in part from the Federal Ministry of Education and Research (BMBF, Germany) in the project NEUROSYS. Helpful discussions with Lucia Reining (École Polytechnique) are gratefully acknowledged. The authors acknowledge the computational resources granted from RWTH Aachen University under project p0020115, as well as JARA0229 and JARA0236. J.Y.R. acknowledges the FNRS CDR project ABIGLO (J.0154.21) as well as support from FNRS and computational resources provided by the CÉCI (funded by the F.R.S.-FNRS under Grant no. 2.5020.11) and the Tier-1 supercomputer of the Fédération Wallonie-Bruxelles (infrastructure funded by the Walloon Region under grant agreement no. 1117545).

Open access funding enabled and organized by Projekt DEAL.

Conflict of Interest

The authors declare no conflict of interest.

Keywords

material design, material maps, metavalent bonding, property predictors, quantum chemical bonding descriptors

Received: September 15, 2022
Revised: October 31, 2022
Published online: March 26, 2023

[1] M. Kulbak, D. Cahen, G. Hodes, *J. Phys. Chem. Lett.* **2015**, *6*, 2452.
[2] M. A. Green, A. Ho-Baillie, H. J. Snaith, *Nat. Photonics* **2014**, *8*, 506.
[3] M. Liu, M. B. Johnston, H. J. Snaith, *Nature* **2013**, *501*, 395.
[4] H.-S. Kim, C.-R. Lee, J.-H. Im, K.-B. Lee, T. Moehl, A. Marchioro, S.-J. Moon, R. Humphry-Baker, J.-H. Yum, J. E. Moser, M. Grätzel, N.-G. Park, *Sci. Rep.* **2012**, *2*, 591.
[5] A. Kojima, K. Teshima, Y. Shirai, T. Miyasaka, *J. Am. Chem. Soc.* **2009**, *131*, 6050.
[6] M. Wuttig, C.-F. Schön, M. Schumacher, J. Robertson, P. Golub, E. Bousquet, C. Gatti, J.-Y. Raty, *Adv. Funct. Mater.* **2022**, *32*, 2110166.
[7] M. I. Eremets, V. S. Minkov, A. P. Drozdov, P. P. Kong, V. Ksenofontov, S. I. Shylin, S. L. Bud'ko, R. Prozorov, F. F. Balakirev, D. Sun, S. Mozaffari, L. Balicas, *J. Supercond. Novel Magn.* **2022**, *35*, 965.
[8] A. Hayat, P. Zareapour, S. Y. F. Zhao, A. Jain, I. G. Savelyev, M. Blumin, Z. Xu, A. Yang, G. D. Gu, H. E. Ruda, S. Jia, R. J. Cava, A. M. Steinberg, K. S. Burch, *Phys. Rev. X* **2012**, *2*, 41019.
[9] C. Felser, X.-L. Qi, *MRS Bull.* **2014**, *39*, 843.
[10] H. J. Snaith, *Nat. Mater.* **2018**, *17*, 372.
[11] M. G. Vergniory, B. J. Wieder, L. Elcoro, S. S. P. Parkin, C. Felser, B. A. Bernevig, N. Regnault, *Science* **2022**, *376*, eabg9094.
[12] M. Wuttig, N. Yamada, *Nat. Mater.* **2007**, *6*, 824.
[13] A. Jain, S. P. Ong, G. Hautier, W. Chen, W. D. Richards, S. Dacek, S. Cholia, D. Gunter, D. Skinner, G. Ceder, K. A. Persson, *APL Mater.* **2013**, *1*, 11002.
[14] S. Curtarolo, W. Setyawan, G. L. Hart, M. Jahnatek, R. V. Chepulskii, R. H. Taylor, S. Wang, J. Xue, K. Yang, O. Levy, M. J. Mehl, H. T. Stokes, D. O. Demchenko, D. Morgan, *Comput. Mater. Sci.* **2012**, *58*, 218.
[15] A. Zunger, *Nat. Rev. Chem.* **2018**, *2*, 0121.
[16] K. Gavroglou, *Neither Physics Nor Chemistry: A History of Quantum Chemistry*, MIT Press, Cambridge, UK **2011**.
[17] L. Pauling, Cornell University, Cornell University Press, *The Nature of the Chemical Bond and the Structure of Molecules and Crystals: An Introduction to Modern Structural Chemistry*, Cornell University Press, Ithaca, NY, USA **1960**.
[18] S. G. Brush, *Stud. Hist. Philos. Sci., Part A* **1999**, *30*, 21.
[19] S. G. Brush, *Stud. Hist. Philos. Sci., Part A* **1999**, *30*, 263.
[20] S. Shaik, P. C. Hiberty, in *Reviews in Computational Chemistry* (Eds: K. B. Lipkowitz, R. Larter, T. R. Cundari), John Wiley & Sons, Ltd., New York **2004**, p. 1.
[21] J. C. Slater, *Phys. Rev.* **1932**, *41*, 255.
[22] J. H. van Vleck, A. Sherman, *Rev. Mod. Phys.* **1935**, *7*, 167.
[23] Walter Kohn Nobel Prize lecture, https://www.nobelprize.org/uploads/2018/06/kohn-lecture.pdf (accessed: November 2022).
[24] J. H. van Vleck, *Phys. Rev.* **1936**, *49*, 232.
[25] Á. M. Pendás, C. Gatti, in *Complementary Bonding Analysis* (Ed: S. Grabowsky), DeGruyter, Boston, MA, USA **2021**.
[26] P. L. A. Popelier, in *Applications of Topological Methods in Molecular Chemistry*, Springer, Cham, Switzerland **2016**, p. 23.
[27] R. F. Bader, *Atoms in Molecules: A Quantum Theory*, Clarendon Press, Oxford, UK **1990**.
[28] C. Gatti, *Z. Kristallogr. – Cryst. Mater.* **2005**, *220*, 399.
[29] C. Gatti, T. R. Cundari, in *Modern Charge-Density Analysis*, (Eds: C. Gatti, P. Macchi), Springer, Dordrecht, The Netherlands **2011**, p. 1.
[30] G. Saleh, D. Ceresoli, G. Macetti, C. Gatti, in *Computational Materials Discovery* (Eds: A. R. Oganov, G. Saleh, A. G. Kvashnin), Royal Society of Chemistry, London, UK **2018**, pp. 117–175.
[31] P. Golub, A. I. Baranov, *J. Chem. Phys.* **2016**, *145*, 154107.
[32] A. I. Baranov, M. Kohout, *J. Comput. Chem.* **2011**, *32*, 2064.
[33] A. Otero-de-la-Roza, E. R. Johnson, V. Luaña, *Comput. Phys. Commun.* **2014**, *185*, 1007.
[34] R. Dronskowski, P. E. Bloechl, *J. Phys. Chem.* **1993**, *97*, 8617.
[35] S. Maintz, V. L. Deringer, A. L. Tchougréeff, R. Dronskowski, *J. Comput. Chem.* **2016**, *37*, 1030.

[36] A. Genoni, L. Bučinský, N. Claiser, J. Contreras-García, B. Dittrich, P. M. Dominiak, E. Espinosa, C. Gatti, P. Giannozzi, J.-M. Gillet, D. Jayatilaka, P. Macchi, A. Ø. Madsen, L. Massa, C. F. Matta, K. M. Merz, P. N. H. Nakashima, H. Ott, U. Ryde, K. Schwarz, M. Sierka, S. Grabowsky, *Chemistry* **2018**, *24*, 10881.
[37] T. S. Koritsanszky, P. Coppens, *Chem. Rev.* **2001**, *101*, 1583.
[38] R. F. Stewart, *Chem. Phys. Lett.* **1979**, *65*, 335.
[39] P. Coppens, *X-Ray Charge Densities and Chemical Bonding*, International Union of Crystallography, New York **1997**.
[40] H. Kasai, K. Tolborg, M. Sist, J. Zhang, V. R. Hathwar, M. Ø. Filsø, S. Cenedese, K. Sugimoto, J. Overgaard, E. Nishibori, B. B. Iversen, *Nat. Mater.* **2018**, *17*, 249.
[41] K. Tolborg, B. B. Iversen, *Chemistry* **2019**, *25*, 15010.
[42] B. D. Dunnington, J. R. Schmidt, *J. Chem. Theory Comput.* **2012**, *8*, 1902.
[43] N. Marzari, A. A. Mostofi, J. R. Yates, I. Souza, D. Vanderbilt, *Rev. Mod. Phys.* **2012**, *84*, 1419.
[44] R. Hoffmann, *Solids and Surfaces: A Chemist's View of Bonding in Extended Structures*, John Wiley & Sons, New York **2002**.
[45] P. Ball, *Nature* **2011**, *469*, 26.
[46] M. L. Cohen, J. R. Chelikowsky, in *Electronic Structure and Optical Properties of Semiconductors*, (Eds: M. Cardona, P. Fulde, K. von Klitzing, H.-J. Queisser), Springer, Berlin/Heidelberg, Germany **1988**, p. 172.
[47] H. Krebs, *Fundamentals of Inorganic Crystal Chemistry*, McGraw-Hill, New York **1968**.
[48] G. Lucovsky, R. M. White, *Phys. Rev. B* **1973**, *8*, 660.
[49] K. Shportko, S. Kremers, M. Woda, D. Lencer, J. Robertson, M. Wuttig, *Nat. Mater.* **2008**, *7*, 653.
[50] J. Hempelmann, P. C. Müller, C. Ertural, R. Dronskowski, *Angew. Chem., Int. Ed.* **2022**, *61*, e202115778.
[51] T. H. Lee, S. R. Elliott, *Adv. Mater.* **2020**, *32*, 2000340.
[52] P. Giannozzi, S. Baroni, N. Bonini, M. Calandra, R. Car, C. Cavazzoni, D. Ceresoli, G. L. Chiarotti, M. Cococcioni, I. Dabo, A. Dal Corso, S. de Gironcoli, S. Fabris, G. Fratesi, R. Gebauer, U. Gerstmann, C. Gougoussis, A. Kokalj, M. Lazzeri, L. Martin-Samos, N. Marzari, F. Mauri, R. Mazzarello, S. Paolini, A. Pasquarello, L. Paulatto, C. Sbraccia, S. Scandolo, G. Sclauzero, A. P. Seitsonen, et al., *J. Phys.: Condens. Matter* **2009**, *21*, 395502.
[53] P. Giannozzi, O. Andreussi, T. Brumme, O. Bunau, M. Buongiorno Nardelli, M. Calandra, R. Car, C. Cavazzoni, D. Ceresoli, M. Cococcioni, N. Colonna, I. Carnimeo, A. Dal Corso, S. de Gironcoli, P. Delugas, R. A. DiStasio, A. Ferretti, A. Floris, G. Fratesi, G. Fugallo, R. Gebauer, U. Gerstmann, F. Giustino, T. Gorni, J. Jia, M. Kawamura, H.-Y. Ko, A. Kokalj, E. Küçükbenli, M. Lazzeri, et al., *J. Phys.: Condens. Matter* **2017**, *29*, 465901.
[54] I. Mayer, *Chem. Phys. Lett.* **1983**, *97*, 270.
[55] K. B. Wiberg, *Tetrahedron* **1968**, *24*, 1083.
[56] P. C. Müller, C. Ertural, J. Hempelmann, R. Dronskowski, *J. Phys. Chem. C* **2021**, *125*, 7959.
[57] R. Hoppe, *Z. Kristallogr. – Cryst. Mater.* **1979**, *150*, 23.
[58] R. F. W. Bader, *Acc. Chem. Res.* **1985**, *18*, 9.
[59] J. G. Angyan, M. Loos, I. Mayer, *J. Phys. Chem.* **1994**, *98*, 5244.
[60] R. L. Fulton, S. T. Mixon, *J. Phys. Chem.* **1993**, *97*, 7530.
[61] J.-Y. Raty, M. Schumacher, P. Golub, V. L. Deringer, C. Gatti, M. Wuttig, *Adv. Mater.* **2019**, *31*, 1806280.
[62] R. Ponec, *J. Math. Chem.* **1997**, *21*, 323.
[63] R. Ponec, *J. Math. Chem.* **1998**, *23*, 85.
[64] W. L. Luken, *Croat. Chem. Acta* **1934**, *57*, 1283.
[65] Y. Cheng, O. Cojocaru-Mirédin, J. Keutgen, Y. Yu, M. Küpers, M. Schumacher, P. Golub, J.-Y. Raty, R. Dronskowski, M. Wuttig, *Adv. Mater.* **2019**, *31*, 1904316.
[66] M. Wuttig, V. L. Deringer, X. Gonze, C. Bichara, J.-Y. Raty, *Adv. Mater.* **2018**, *30*, 1803777.
[67] A. Heßler, S. Wahl, T. Leuteritz, A. Antonopoulos, C. Stergianou, C.-F. Schön, L. Naumann, N. Eicker, M. Lewin, T. W. W. Maß, M. Wuttig, S. Linden, T. Taubner, *Nat. Commun.* **2021**, *12*, 924.
[68] G. N. Lewis, *J. Am. Chem. Soc.* **1916**, *38*, 762.
[69] I. Langmuir, *J. Am. Chem. Soc.* **1919**, *41*, 868.
[70] A. E. van Arkel, *Molecules and Crystals in Inorganic Chemistry*, Interscience Publishers, New York **1956**.
[71] J. A. A. Ketelaar, *Chemical Constitution: An Introduction to the Theory of the Chemical Bond*, Amsterdam, The Netherlands **1958**.
[72] B. J. Kooi, M. Wuttig, *Adv. Mater.* **2020**, *32*, 1908302.
[73] P. B. Littlewood, *J. Phys. C: Solid State Phys.* **1980**, *13*, 4855.
[74] J. John, A. N. Bloch, *Phys. Rev. Lett.* **1974**, *33*, 1095.
[75] G. Simons, A. N. Bloch, *Phys. Rev. B* **1973**, *7*, 2754.
[76] J. C. Phillips, *Solid State Commun.* **1977**, *22*, 549.
[77] J. R. Chelikowsky, J. C. Phillips, *Phys. Rev. B* **1978**, *17*, 2453.
[78] H. Ibach, H. Lüth, *Solid-State Physics: An Introduction to Principles of Materials Science*, Springer, Berlin/Heidelberg, Germany **2009**.
[79] J.-Y. Raty, M. Wuttig, *J. Phys. D: Appl. Phys.* **2020**, *53*, 234002.
[80] C.-F. Schön, S. van Bergerem, C. Mattes, A. Yadav, M. Grohe, L. Kobbelt, M. Wuttig, *Sci. Adv.* **2022**, *8*, eade0828.
[81] S. Maier, S. Steinberg, Y. Cheng, C.-F. Schön, M. Schumacher, R. Mazzarello, P. Golub, R. Nelson, O. Cojocaru-Mirédin, J.-Y. Raty, M. Wuttig, *Adv. Mater.* **2020**, *32*, 2005533.
[82] E. Fermi, *Nuclear Physics*, Univ. of Chicago Press, Chicago **1974**.
[83] P. A. M. Dirac, *Proc. R. Soc. London, Ser. A* **1927**, *114*, 243.
[84] M. K. Brod, M. Y. Toriyama, G. J. Snyder, *Chem. Mater.* **2020**, *32*, 9771.
[85] M. Cagnoni, D. Führen, M. Wuttig, *Adv. Mater.* **2018**, *30*, 1801787.
[86] P. B. Littlewood, *J. Phys. C: Solid State Phys.* **1980**, *13*, 4875.
[87] J. E. Jaffe, A. Zunger, *Phys. Rev. B* **1983**, *28*, 5822.
[88] H. Neumann, *Cryst. Res. Technol.* **1983**, *18*, 901.
[89] A. Zunger, J. E. Jaffe, *Phys. Rev. Lett.* **1983**, *51*, 662.
[90] J. E. Jaffe, A. Zunger, *Phys. Rev. B* **1984**, *29*, 1882.
[91] M. Buffiere, D. S. Dhawale, F. El-Mellouhi, *Energy Technol.* **2019**, *7*, 1900819.
[92] R. Scheer, *Chalcogenide Photovoltaics: Physics, Technologies, and Thin Film Devices*, John Wiley & Sons Incorporated, Weinheim, Germany **2008**.
[93] D. B. Mitzi, in *Progress in Inorganic Chemistry*, (Ed: K. D. Karlin), John Wiley & Sons, Ltd., New York **2007**, p. 1.
[94] M. M. Lee, J. Teuscher, T. Miyasaka, T. N. Murakami, H. J. Snaith, *Science* **2012**, *338*, 643.
[95] S. Raoux, W. Wełnic, D. Ielmini, *Chem. Rev.* **2010**, *110*, 240.
[96] N. I. Zheludev, *J. Opt. A: Pure Appl. Opt.* **2006**, *8*, S1.
[97] M. Wuttig, H. Bhaskaran, T. Taubner, *Nat. Photonics* **2017**, *11*, 465.
[98] B. Huang, J. Robertson, *Phys. Rev. B* **2010**, *81*, 81204.
[99] G. Bruns, P. Merkelbach, C. Schlockermann, M. Salinga, M. Wuttig, T. D. Happ, J. B. Philipp, M. Kund, *Appl. Phys. Lett.* **2009**, *95*, 43108.
[100] W. Zhang, R. Mazzarello, M. Wuttig, E. Ma, *Nat. Rev. Mater.* **2019**, *4*, 150.
[101] D. Loke, T. H. Lee, W. J. Wang, L. P. Shi, R. Zhao, Y. C. Yeo, T. C. Chong, S. R. Elliott, *Science* **2012**, *336*, 1566.
[102] C. Persch, M. J. Müller, A. Yadav, J. Pries, N. Honné, P. Kerres, S. Wei, H. Tanaka, P. Fantini, E. Varesi, F. Pellizzer, M. Wuttig, *Nat. Commun.* **2021**, *12*, 4978.
[103] P. G. Debenedetti, F. H. Stillinger, *Nature* **2001**, *410*, 259.
[104] Y. Yu, M. Cagnoni, O. Cojocaru-Mirédin, M. Wuttig, *Adv. Funct. Mater.* **2020**, *30*, 1904862.
[105] S. Shaik, D. Danovich, J. M. Galbraith, B. Braïda, W. Wu, P. C. Hiberty, *Angew. Chem., Int. Ed.* **2020**, *59*, 984.
[106] J. K. Burdett, *Chemical Bonding in Solids*, Oxford University Press, Oxford **1995**.
[107] M. Zhu, O. Cojocaru-Mirédin, A. M. Mio, J. Keutgen, M. Küpers, Y. Yu, J.-Y. Cho, R. Dronskowski, M. Wuttig, *Adv. Mater.* **2018**, *30*, 1706735.

[108] L. Guarneri, S. Jakobs, A. von Hoegen, S. Maier, M. Xu, M. Zhu, S. Wahl, C. Teichrib, Y. Zhou, O. Cojocaru-Mirédin, M. Raghuwanshi, C.-F. Schön, M. Drögeler, C. Stampfer, R. P. S. M. Lobo, A. Piarristeguy, A. Pradel, J.-Y. Raty, M. Wuttig, *Adv. Mater.* **2021**, *33*, 2102356.
[109] M. Raghuwanshi, O. Cojocaru-Mirédin, M. Wuttig, *Nano Lett.* **2020**, *20*, 116.
[110] *Numerical Data and Functional Relationships in Science and Technology: New Series*, Vol. *41C* (Eds: O. Madelung, U. Rössler, M. Schulz, O. Madelung, R. Clasen, H. Landolt, R. Börnstein, W. Martienssen), Springer, Berlin, Germany **1998**, p. 1.
[111] R. Bochicchio, R. Ponec, A. Torre, L. Lain, *Theor. Chem. Acc.* **2001**, *105*, 292.
[112] C. E. Housecroft, A. G. Sharpe, *Inorganic Chemistry*, Pearson, London, UK **2012**.
[113] S. Shaik, D. Danovich, J. M. Galbraith, B. Braïda, W. Wu, P. C. Hiberty, *Angew. Chem., Int. Ed.* **2020**, *59*, 984.
[114] D. Kim, *personal communication*.
[115] A. Gallo-Bueno, M. Kohout, E. Francisco, Á. Martín Pendás, *J. Chem. Theory Comput.* **2022**, *18*, 4245.
[116] Y. Luo, Z. Ma, S. Hao, S. Cai, Z.-Z. Luo, C. Wolverton, V. P. Dravid, J. Yang, Q. Yan, M. G. Kanatzidis, *J. Am. Chem. Soc.* **2022**, *144*, 1445.
[117] D. Sarkar, S. Roychowdhury, R. Arora, T. Ghosh, A. Vasdev, B. Joseph, G. Sheet, U. V. Waghmare, K. Biswas, *Angew. Chem., Int. Ed.* **2021**, *60*, 10350.
[118] C. Rodenkirchen, M. Cagnoni, S. Jakobs, Y. Cheng, J. Keutgen, Y. Yu, M. Wuttig, O. Cojocaru-Mirédin, *Adv. Funct. Mater.* **2020**, *30*, 1910039.
[119] M. Al-Fahdi, X. Zhang, M. Hu, *J. Mater. Sci.* **2021**, *56*, 18534.
[120] L. Elalfy, D. Music, M. Hu, *Phys. Rev. B* **2021**, *103*, 75203.
[121] K. Tolborg, B. B. Iversen, *Chem. Mater.* **2021**, *33*, 5308.
[122] K. A. U. Holm, N. Roth, C. M. Zeuthen, K. Tolborg, A. A. Feidenhans'l, B. B. Iversen, *Phys. Rev. B* **2020**, *102*, 24112.
[123] K. A. U. Holm, N. Roth, C. M. Zeuthen, B. B. Iversen, *Phys. Rev. B* **2021**, *103*, 224302.
[124] A. M. Mio, P. M. Konze, A. Meledin, M. Küpers, M. Pohlmann, M. Kaminski, R. Dronskowski, J. Mayer, M. Wuttig, *Adv. Funct. Mater.* **2019**, *29*, 1902332.
[125] P. Noé, A. Verdy, F. d'Acapito, J.-B. Dory, M. Bernard, G. Navarro, J.-B. Jager, J. Gaudin, J.-Y. Raty, *Sci. Adv.* **2020**, *6*, eaay2830.
[126] W. J. Yang, T. Ha, B. C. Park, K.-S. Jeong, J. Y. Park, D. Kim, C. Lee, J. Park, M.-H. Cho, *ACS Nano* **2022**, *16*, 2024.
[127] V. P. Cuenca-Gotor, J. Á. Sans, O. Gomis, A. Mujica, S. Radescu, A. Muñoz, P. Rodríguez-Hernández, E. L. Da Silva, C. Popescu, J. Ibañez, R. Vilaplana, F. J. Manjón, *Phys. Chem. Chem. Phys.* **2020**, *22*, 3352.
[128] N. V. Morozova, I. V. Korobeynikov, N. Miyajima, S. V. Ovsyannikov, *Adv. Sci.* **2022**, *9*, e2103720.
[129] J. A. Sans, R. Vilaplana, E. L. Da Silva, C. Popescu, V. P. Cuenca-Gotor, A. Andrada-Chacón, J. Sánchez-Benitez, O. Gomis, A. L. J. Pereira, P. Rodríguez-Hernández, A. Muñoz, D. Daisenberger, B. García-Domene, A. Segura, D. Errandonea, R. S. Kumar, O. Oeckler, P. Urban, J. Contreras-García, F. J. Manjón, *Inorg. Chem.* **2020**, *59*, 9900.
[130] C. Bellin, A. Pawbake, L. Paulatto, K. Béneut, J. Biscaras, C. Narayana, A. Polian, D. J. Late, A. Shukla, *Phys. Rev. Lett.* **2020**, *125*, 145301.
[131] F. J. Manjón, J. Á. Sans, P. Rodríguez-Hernández, A. Muñoz, *Minerals* **2021**, *11*, 1283.
[132] S. Sun, L. Zhu, W. Zhang, *Phys. Status Solidi RRL* **2022**, *16*, 2100626.
[133] A. Edwards, A. Pineda, P. Schultz, M. Martin, A. Thompson, H. Hjalmarson, C. Umrigar, *Phys. Rev. B* **2006**, *73*, 45210.
[134] T. Siegrist, P. Jost, H. Volker, M. Woda, P. Merkelbach, C. Schlockermann, M. Wuttig, *Nat. Mater.* **2011**, *10*, 202.
[135] W. Zhang, A. Thiess, P. Zalden, R. Zeller, P. H. Dederichs, J.-Y. Raty, M. Wuttig, S. Blügel, R. Mazzarello, *Nat. Mater.* **2012**, *11*, 952.
[136] K. S. Siegert, F. R. L. Lange, E. R. Sittner, H. Volker, C. Schlockermann, T. Siegrist, M. Wuttig, *Rep. Prog. Phys.* **2015**, *78*, 13001.
[137] J. Reindl, H. Volker, N. P. Breznay, M. Wuttig, *npj Quantum Mater.* **2019**, *4*, 57.
[138] I. Korzhovska, H. Deng, L. Zhao, Y. Deshko, Z. Chen, M. Konczykowski, S. Zhao, S. Raoux, L. Krusin-Elbaum, *npj Quantum Mater.* **2020**, *5*, 39.
[139] Y. Xu, X. Wang, W. Zhang, L. Schäfer, J. Reindl, F. vom Bruch, Y. Zhou, V. Evang, J.-J. Wang, V. L. Deringer, E. Ma, M. Wuttig, R. Mazzarello, *Adv. Mater.* **2021**, *33*, 2006221.
[140] D. Giri, L. Williams, A. Mukherjee, K. Rajan, *J. Chem. Phys.* **2021**, *154*, 124105.
[141] H. H. H. Osman, F. J. Manjón, *Phys. Chem. Chem. Phys.* **2022**, *24*, 9936.
[142] Y. Wu, P. Qiu, Y. Yu, Y. Xiong, T. Deng, O. Cojocaru-Mirédin, M. Wuttig, X. Shi, L. Chen, *J. Materiomics* **2022**, *8*, 1095.
[143] M. Küpers, P. M. Konze, S. Maintz, S. Steinberg, A. M. Mio, O. Cojocaru-Mirédin, M. Zhu, M. Müller, M. Luysberg, J. Mayer, M. Wuttig, R. Dronskowski, *Angew. Chem., Int. Ed.* **2017**, *56*, 10204.
[144] K. Momma, F. Izumi, *J. Appl. Crystallogr.* **2008**, *41*, 653.
[145] N. N. Greenwood, *Chemistry of the Elements*, Elsevier-Butterworth-Heinemann, Amsterdam, The Netherlands **2010**.
[146] *CRC Handbook of Chemistry and Physics: A Ready-Reference Book of Chemical and Physical Data* (Eds: W. M. Haynes, D. R. Lide), CRC Press; Taylor & Francis, Boca Raton, FL; London, UK **2011**.
[147] R. E. Bedford, G. Bonnier, H. Maas, F. Pavese, *Metrologia* **1996**, *33*, 133.

Matthias Wuttig received his Ph.D. in physics in 1988 from RWTH Aachen/Forschungszentrum Jülich. He was a visiting professor at several institutions including Lawrence Berkeley Laboratory, CINaM (Marseille), Stanford University, Hangzhou University, IBM Almaden, Bell Labs, DSI in Singapore, and the Chinese Academy of Sciences in Shanghai. In 1997, he was appointed full professor at RWTH Aachen. Since 2011, he has been heading a collaborative research center on resistively switching chalcogenides (SFB 917), funded by the DFG.

Carl-Friedrich Schön received his B.S. and M.S. in physics at the RWTH Aachen University, Germany. He is currently enrolled as a Ph.D. student at the I. Institute of Physics (IA), RWTH Aachen University and has spent semesters at the University of Tokyo (東京大学), Japan and the Nanyang Technological University (NTU) in Singapore. His research interests are density functional theory (DFT), quantum theory of atoms in molecules (QTAIM), and machine learning (ML).

Jakob Lötfering is currently pursuing his Ph.D. in the I. Institute of Physics at the RWTH Aachen University. He received his bachelor's degree in physics from the TU Dresden and his master's degree from the University of Göttingen, where he specialized in theoretical physics. His current research interests lie in new photovoltaic materials, metavalent bonding, and the QTAIM.

Pavlo Golub obtained his Ph.D. degree in chemistry in 2017 from Technical University Dresden. Since then he worked as research fellow at National University of Singapore and at J. Heyrovsky Institute of Physical Chemistry, Prague. His main interests are properties of strongly correlated systems and development of accurate quantum-chemical methods for material research.

Carlo Gatti received (1978) his degree in chemistry/theoretical/physical/chemistry from Milano University. He was (now retired) research Director at CNR-SCITEC, Milano. As expert of quantum chemical topology (QCT) methods, he has applied them to chemical bonding in crystals/solids/materials, using ab initio and X-ray-derived experimental data and devising novel QCT descriptors. He is author/co-author of worldwide distributed QCT codes. Among others, he cooperated with R. Bader, B. Silvi, A. M. Pendas, P. Coppens, B. B. Iversen, A. Oganov, and recently with M. Wuttig. Along with Mark Spackman, he was awarded the Gregori Aminoff 2013 prize for crystallography by the Royal Swedish Academy of Science.

Jean-Yves Raty obtained a Ph.D. in physics in 1999 from the University of Liège in Belgium. After having held postdoctoral positions at the Lawrence Livermore National Laboratory and by the Belgian FNRS, he became a permanent researcher, then senior research associate (FNRS), in Liège. An invited professor at the CEA-Leti Grenoble and Institut Lumière Matière in U. Lyon, he is now heading the Condensed Matter Simulation Group at the University of Liège, with a focus on amorphous and liquid materials.